

# Eddington ratios of faint AGN at intermediate redshift: evidence for a population of half-starved black holes<sup>★</sup>

I. Gavignaud<sup>1</sup>, L. Wisotzki<sup>1</sup>, A. Bongiorno<sup>2</sup>, S. Paltani<sup>3,4</sup>, G. Zamorani<sup>5</sup>, P. Møller<sup>6</sup>, V. Le Brun<sup>7</sup>, B. Husemann<sup>1</sup>, F. Lamareille<sup>8</sup>, M. Schramm<sup>1</sup>, O. Le Fèvre<sup>7</sup>, D. Bottini<sup>9</sup>, B. Garilli<sup>9</sup>, D. Maccagni<sup>9</sup>, R. Scaramella<sup>10,11</sup>, M. Scoggio<sup>9</sup>, L. Tresse<sup>7</sup>, G. Vettolani<sup>10</sup>, A. Zanichelli<sup>10</sup>, C. Adami<sup>7</sup>, M. Arnaboldi<sup>12</sup>, S. Arnouts<sup>7</sup>, S. Bardelli<sup>5</sup>, M. Bolzonella<sup>5</sup>, A. Cappi<sup>5</sup>, S. Charlot<sup>13</sup>, P. Ciliegi<sup>5</sup>, T. Contini<sup>8</sup>, S. Foucaud<sup>14</sup>, P. Franzetti<sup>9</sup>, L. Guzzo<sup>15</sup>, O. Ilbert<sup>16</sup>, A. Iovino<sup>15</sup>, H. J. McCracken<sup>13,17</sup>, B. Marano<sup>18</sup>, C. Marinoni<sup>8</sup>, A. Mazure<sup>8</sup>, B. Meneux<sup>9,15</sup>, R. Merighi<sup>5</sup>, R. Pellò<sup>8</sup>, A. Pollo<sup>8</sup>, L. Pozzetti<sup>5</sup>, M. Radovich<sup>12</sup>, E. Zucca<sup>5</sup>, M. Bondi<sup>10</sup>, G. Busarello<sup>12</sup>, O. Cucciati<sup>15,18</sup>, S. de la Torre<sup>8</sup>, L. Gregorini<sup>10</sup>, Y. Mellier<sup>13,17</sup>, P. Merluzzi<sup>12</sup>, V. Ripepi<sup>12</sup>, D. Rizzo<sup>2</sup>, and D. Vergani<sup>9</sup>

<sup>1</sup> Astrophysikalisches Institut Potsdam, An der Sternwarte 16, 14482 Potsdam, Germany  
e-mail: igavignaud@aip.de

<sup>2</sup> Max-Planck-Institut für Extraterrestrische Physik, Giessenbachstr., 85741 Garching, Germany

<sup>3</sup> Integral Science Data Centre, Ch. d'Écogia 16, 1290 Versoix, Switzerland

<sup>4</sup> Geneva Observatory, Ch. des Maillettes 51, 1290 Sauverny, France

<sup>5</sup> INAF-Osservatorio Astronomico di Bologna, via Ranzani, 1, 40127, Bologna, Italy

<sup>6</sup> European Southern Observatory, Karl-Schwarzschild-Strasse 2, 85748 Garching bei München, Germany

<sup>7</sup> Laboratoire d'Astrophysique de Marseille (UMR6110), CNRS-Université de Provence, 38 rue Frederic Joliot-Curie, 13388 Marseille Cedex 13, France

<sup>8</sup> Laboratoire d'Astrophysique de Toulouse-Tarbes, Université de Toulouse, CNRS, 14 avenue Édouard Belin, 31400 Toulouse, France

<sup>9</sup> IASF-INAF, via Bassini 15, 20133, Milano, Italy

<sup>10</sup> IRA-INAF, via Gobetti, 101, 40129, Bologna, Italy

<sup>11</sup> INAF-Osservatorio Astronomico di Roma, via di Frascati 33, 00040 Monte Porzio Catone, Italy

<sup>12</sup> INAF-Osservatorio Astronomico di Capodimonte, via Moiariello 16, 80131 Napoli, Italy

<sup>13</sup> Institut d'Astrophysique de Paris, UMR 7095, 98bis Blvd. Arago, 75014 Paris, France

<sup>14</sup> School of Physics & Astronomy, University of Nottingham, University Park, Nottingham, NG72RD, UK  
INAF-Osservatorio Astronomico di Brera, via Brera 28, Milan, Italy

<sup>15</sup> Canada France Hawaii Telescope corporation, Mamalahoa Hwy, Kamuela, 96743, USA

<sup>16</sup> Observatoire de Paris, LERMA, 61 avenue de l'Observatoire, 75014 Paris, France

<sup>17</sup> Università di Bologna, Dipartimento di Astronomia, via Ranzani, 1, 40127, Bologna, Italy

<sup>18</sup> Università di Milano-Bicocca, Dipartimento di Fisica, Piazza delle Scienze, 3, 20126 Milano, Italy

Received 29 October 2007 / Accepted 17 October 2008

## ABSTRACT

We use one of the deepest spectroscopic samples of broad-line active galactic nuclei (AGN) currently available, extracted from the VIMOS VLT Deep Survey (VVDS), to compute the Mg II and C IV virial-mass estimates of 120 super-massive black holes in the redshift range  $1.0 < z < 1.9$  and  $2.6 < z < 4.3$ . We find that the mass-luminosity relation shows considerably enhanced dispersion towards low AGN luminosities ( $\log L_{\text{bol}} \sim 45$ ). At these luminosities, there is a substantial fraction of black holes accreting far below their Eddington limit ( $L_{\text{bol}}/L_{\text{Edd}} < 0.1$ ), in marked contrast to what is generally found for AGN of higher luminosities. We speculate that these may be AGN on the decaying branch of their lightcurves, well past their peak activity. This would agree with recent theoretical predictions of AGN evolution. In the electronic Appendix of this paper we publish an update of the VVDS type-1 AGN sample, including the first and most of the second-epoch observations. This sample contains 298 objects of which 168 are new.

**Key words.** galaxies: active – galaxies: Seyfert – galaxies: nuclei

## 1. Introduction

The mass scaling relations of super-massive black holes in present-day galaxies (e.g., Gebhardt et al. 2000; Ferrarese & Merritt 2000) imply that black hole growth must be closely

connected to the overall formation and evolution of galaxies. Most of the mass locked up in black holes today was probably accumulated through accretion in discrete phases of nuclear activity, as suggested by the consistency between the estimate of the black hole mass density at  $z \approx 0$  and that derived from the integrated AGN luminosity density (Soltan 1982; Yu & Tremaine 2002; Marconi et al. 2004).

\* Based on data obtained with the European Southern Observatory Very Large Telescope, Paranal, Chile, program 070.A-9007(A), 272.A-5047, 076.A-0808, and partially on data obtained at the Canada-France-Hawaii Telescope.

Accretion histories of individual black holes are essentially unconstrained by observations. By looking at AGN one may at least catch snapshots of the black hole growth process, especially when black hole masses and thus accretion rates can be estimated. There has been significant progress in this direction over the past years, and it has been demonstrated that single-epoch spectroscopic and photometric measurements of AGN with broad emission lines (type 1 AGN) allow one to estimate black hole masses to an accuracy on the order of  $\pm 0.5$  dex (Vestergaard 2002; McLure & Jarvis 2002; Collin et al. 2006). With this approach it has been possible to explore the distribution of Eddington ratios for large AGN surveys (McLure & Dunlop 2004; Kollmeier et al. 2006).

These studies have shown that powerful type 1 AGN appear to accrete at rates close to the Eddington limit with remarkable uniformity, and yet periods of activity must be followed by a transition from high-luminosity, near-Eddington states to almost quiescent black holes. Unless this transition is rather abrupt, there should also be a population of AGN with significantly lower Eddington ratios, but still recognizable as bona fide AGN. We report on observations of such a population at intermediate redshifts, based on black hole mass estimates that we derive for a new sample of faint AGN with complete spectroscopic identification.

In this work, absolute luminosities are computed assuming a flat universe with cosmological parameters  $\Omega_m = 0.3$ ,  $\Omega_\Lambda = 0.7$ , and  $H_0 = 70 \text{ km s}^{-1}$ .

## 2. The sample

The VVDS (VLT-VIMOS Deep Survey) is a purely  $I$ -band flux limited spectroscopic survey designed to study the evolution of galaxies, AGN, and large-scale structure. It comprises two subsets: a “deep” survey with a limit of  $I_{AB} \leq 24$  (Le Fèvre et al. 2005) and a “wide” and a shallower survey with  $I_{AB} \leq 22.5$  (Garilli et al. 2008). Both surveys utilize the VIMOS multi-object spectrograph on the ESO-VLT to take spectra of objects above the flux limit, irrespective of their morphological properties or colors, albeit with a sparse target sampling rate (for details see the above-mentioned papers).

About 1% of all VVDS targets can be classified as type 1 AGN on the basis of their broad emission lines. From the VVDS we can therefore construct AGN samples that have two advantages over most other surveys. (i) The very faint limiting magnitude, which is even deeper than that of the multi-color photometric COMBO-17 survey (Wolf et al. 2003); and (ii) the simple selection criterion, which only requires the presence of a broad emission line ( $FWHM \geq 1000 \text{ km s}^{-1}$ ) in any given spectrum. This way, we recently constructed a well-defined sample of type 1 AGN, which is described in detail by Gavignaud et al. (2006). In that paper we demonstrated that, since the sample is unaffected by morphological or color pre-selection biases, it is also much less prone to incompleteness due to host galaxy contamination. The sample has already been used to investigate the AGN luminosity function and its evolution (Bongiorno et al. 2007). Here we exploit the spectroscopic properties of that sample, containing 130 broad-line AGN, supplemented by 168 AGN of the VVDS second epoch data. The merged updated catalog of AGN is published in Appendix B of this paper. It contains 222 and 76 AGN from the “wide” and the “deep” survey respectively. The median redshift is  $z \sim 1.8$  (roughly equal for the wide and deep subsets), with a broad distribution of redshifts within  $1 \leq z \leq 3$ .

## 3. Black hole masses and Eddington ratios

In order to estimate the black hole masses in type 1 AGN from single epoch spectroscopy, it must be assumed that the line-emitting “clouds” are roughly in virial equilibrium, and that the size of the broad-line region (BLR) is closely correlated with the luminosity of the AGN. The black hole mass is then given by the virial relation (Collin et al. 2006),  $M_{\text{BH}} = f(R\Delta V^2)/G$ , where  $G$  is the gravitational constant,  $R$  is the size of the BLR, which in turn is estimated from the continuum luminosity,  $f$  is a dimensionless factor close to unity which reflects the unknown geometry and inclination of the BLR, and  $\Delta V$  represents the velocity broadening of a given broad emission line.  $\Delta V$  can be estimated using either the line  $FWHM$  or the line velocity dispersion  $\sigma_1$ .

We have applied this approach to our sample of 298 type 1 AGN. The spectral range available for measuring line widths is 5700 Å–8200 Å. Consequently, for  $1.0 \leq z \leq 1.9$ , the spectra contain the Mg II  $\lambda 2798$  emission line, while C IV  $\lambda 1550$  is accessible for  $2.6 \leq z \leq 4.3$ .

In the case of Mg II, we applied an iterative procedure to subtract the Fe II contamination from the AGN continuum using a template kindly provided by Vestergaard (see Vestergaard & Wilkes 2001). Since this template is derived from the observed spectrum of a narrow line Seyfert I, it is difficult to deblend the Fe II pseudo-continuum emission from other emission lines. In particular, the template contains no flux under the Mg II line itself although some amount of flux is expected from theoretical models (Sigut & Pradhan 2003). The effect of adding flux to the empirical template has been recently quantified by Fine et al. (2008) and is found to be negligible in view of the other errors. In this work we used the unmodified template.

The Mg II and C IV emission line profiles were modeled by a superposition of two Gaussian components; the line widths were obtained from these fits. The measurements were then corrected for the finite spectrograph resolution assuming that  $\Delta\lambda_{\text{obs}}^2 = \Delta\lambda_{\text{intrinsic}}^2 + \Delta\lambda_{\text{res}}^2$ . The mean instrumental resolution of the VVDS spectra corresponds to  $\Delta\sigma_{\text{res}} = 350 \text{ km s}^{-1}$ . Errors on the velocity measurements are obtained by combining the nominal errors of the fit parameters and the uncertainties due to the adopted continuum level. Figure 1 shows two examples of fits to the spectra (continuum + emission lines) representative for the two redshift intervals.

Objects with a mean signal-to-noise ( $S/N$ ) ratio per pixel lower than 7, in the vicinity of the emission line, were excluded from further analysis (this concerns 8 Mg II and 8 C IV objects). 20 of the high-redshift C IV line profiles and 4 of the low-redshift Mg II were heavily affected by associated absorption or instrumental problems, and these were also eliminated. After these cuts we remained with a sample of 120 objects, 91 of which feature the Mg II, and 29 of which feature the C IV line. The median redshift is 1.5 for the Mg II subsample and 3.1 for the C IV subsample, respectively.

We flux-calibrated our spectra by scaling them to the  $I$  band photometry in the CFHT images used as input to the VVDS. Monochromatic luminosities at given rest-frame wavelengths were then directly measured from the spectra.

In order to apply the virial relation to measurements of the Mg II emission line we used the empirical calibration by McLure & Dunlop (2004)

$$\log \frac{M_{\text{BH}}}{M_\odot} = \log \left( FWHM_{1000}^2 ((\lambda L)_{443\,000})^{0.62} \right) + 6.51 \quad (1)$$

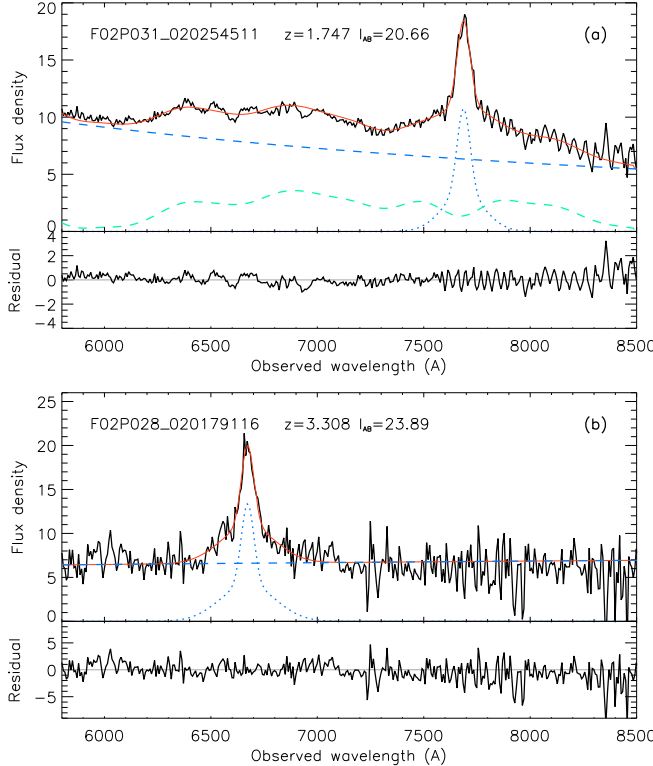


**Fig. 1.** Two examples of emission line fits to the spectra. In **a**) we show an object from our low-redshift sample with the Mg II line and in **b**) an example of the high-redshift sample with the C IV line. The observed spectra are displayed in black, the fits are overplotted in red. Each fit is a combination of a power-law continuum (blue dashed line), a double-Gaussian model of the broad emission line (blue dotted line) and, only for the Mg II sample, a broadened empirical template of the Fe II pseudo-continuum emission (green dashed-line).

where  $FWHM_{1000}$  is the  $FWHM$  of the line in units of  $1000 \text{ km s}^{-1}$ , and  $\lambda L_{443\,000}$  is the monochromatic luminosity at  $\lambda = 3000 \text{ Å}$ , expressed in units of  $10^{44} \text{ erg s}^{-1}$ .

For AGN where only C IV could be measured, we employed the recent relation by Vestergaard & Peterson (2006),

$$\log \frac{M_{\text{BH}}}{M_{\odot}} = \log \left( \sigma_{1000}^2 (\lambda L)_{44,1350}^{0.53} \right) + 6.73 \quad (2)$$

where  $\sigma_{1000}$  is the emission line velocity dispersion in units of  $1000 \text{ km s}^{-1}$  and  $(\lambda L)_{44,1350}$  is the monochromatic luminosity at  $1350 \text{ Å}$ , expressed in units of  $10^{44} \text{ erg s}^{-1}$ .

Bolometric luminosities were derived from the monochromatic ones, multiplied by a correction factor  $f_{\text{bol}}$ . It is now established that, on average, at UV and optical wavelengths this correction factor increases towards lower luminosities (e.g. Richards et al. 2006; Steffen et al. 2006). Hopkins et al. (2007) provide an empirical model of AGN SED which varies with bolometric luminosity and is calibrated from a large number of observational studies<sup>1</sup>. Following this model,  $f_{\text{bol}}(3000 \text{ Å})$  decreases from 6.8 to 5.6 over the luminosity range  $\log L_{\text{bol}} = [44.8, 46.2]$ , while  $f_{\text{bol}}(1350 \text{ Å})$  varies between 4.2 and 3.7 for  $\log L_{\text{bol}} = [45.2, 46.4]$ .

Together with black hole masses and bolometric luminosities we also estimated the dimensionless “Eddington ratios”

$\epsilon = L_{\text{bol}}/L_{\text{Edd}}$ , where  $L_{\text{Edd}}$  is the Eddington luminosity of the black hole assuming spherically symmetric accretion.

## 4. Results

The distribution of the inferred BH masses versus bolometric luminosities is shown Fig. 2a. As expected, there is a trend of  $M_{\text{BH}}$  increasing with  $L_{\text{bol}}$ . The overall mean and associated error of the BH masses for the full sample is  $\log M_{\text{BH}} = 8.28 \pm 0.04$ . We split our sample at  $\log L = 45.7$  into a “low luminosity” and a “high luminosity” subset, containing respectively 62 and 58 objects. The corresponding mean BH masses are  $8.00 \pm 0.05$  and  $8.57 \pm 0.04$ , respectively. However, the trend is not consistent with the assumption of  $L_{\text{bol}} \propto M_{\text{BH}}$ , i.e. with an Eddington ratio  $\epsilon$  independent of AGN luminosity. This is highlighted in Fig. 2b, where we plot  $\epsilon$  versus  $L_{\text{bol}}$  for the same objects. The mean  $\log \epsilon$  for the full sample is  $-0.71 \pm 0.03$  and has a dispersion of 0.33 dex. For the “low luminosity” sample the mean is  $\log \epsilon = -0.81 \pm 0.04$ , and for the “high luminosity” subset  $\log \epsilon = -0.61 \pm 0.03$ .

The dispersion of  $\epsilon$  differs even more strongly between low and high luminosity subsets: for  $\log L_{\text{bol}} > 45.7$ , there is little spread in  $\epsilon$  (1st and 3rd quartiles in  $\log \epsilon$  are  $-0.79$  and  $-0.44$ ). For  $\log L_{\text{bol}} < 45.7$ , however, the spread is larger, with 1st and 3rd quartiles being  $-1.06$  and  $-0.55$ , respectively. A similar behavior is observed for other percentiles. A Kolmogorov-Smirnov test comparing the distribution of  $\epsilon$  in the two subsets gives a probability of only 1.8% that both subsets were drawn from the same parent population; thus, the two subsets have significantly different distributions in their Eddington ratios.

Most of the difference between the two  $\epsilon$  distributions is due to the existence of a significant tail of low  $\epsilon$  values for the low luminosity AGN. In fact, the fraction of slowly accreting black holes with  $\epsilon < 0.1$  for the AGN with  $\log L_{\text{bol}} < 45.7$  (16/62) is five times larger than the same fraction for those with  $\log L_{\text{bol}} > 45.7$  (3/58). The significance of the difference in this tail, derived on the basis of a Fisher exact test on a  $2 \times 2$  contingency table, is at about the  $3\sigma$  level.

The large number of low- $\epsilon$  AGN at low luminosities produces an apparent trend of  $\epsilon$  increasing with  $L_{\text{bol}}$ . A formal regression gives  $\log \epsilon = -0.89 + 0.30 (\log L_{\text{bol}} - 45)$ . We caution however against an overinterpretation of that trend, as our sample covers only a limited range of luminosities. A much wider luminosity range would be needed to establish a robust  $\epsilon(L_{\text{bol}})$  relation (but see the discussion in Sect. 5.1 and Fig. 4). Moreover, as also discussed below, the slope of this relations depends on the choice of the exponent of the empirical luminosity-size relation adopted in the virial scaling relations. The linear-Pearson ( $r$ ) and Spearman-rank ( $\rho$ ) correlation coefficients between  $\log L_{\text{bol}}$  and  $\log \epsilon$  taken alone indicate a mild correlation ( $r = 0.40$  and  $\rho = 0.37$ , respectively).

About 75% of the AGN in our sample belong to the low-redshift, Mg II subsample at an average redshift of  $\sim 1.5$ . Since higher redshift AGN in the sample have, on average, higher luminosities, the C IV sample is populating mostly the “high luminosity” region of Fig. 2. In the overlapping luminosity range ( $45.5 \lesssim \log L_{\text{bol}} \lesssim 46.4$ ), the AGN in the two redshift intervals have similar mean Eddington ratios or BH masses. However the high redshift objects seem to follow a steeper and tighter  $\log \epsilon = \alpha \log L_{\text{bol}} + \text{const.}$  relation ( $\alpha = 0.40$ ,  $r = 0.75$ ) than the low redshift sample ( $\alpha = 0.22$ ,  $r = 0.24$ ). Interestingly, the difference in the best fit slope  $\alpha$  between the two subsamples disappears if one adopts scaling relations with the same

<sup>1</sup> See

<http://www.cfa.harvard.edu/~phopkins/Site/qlf.html> and references therein.

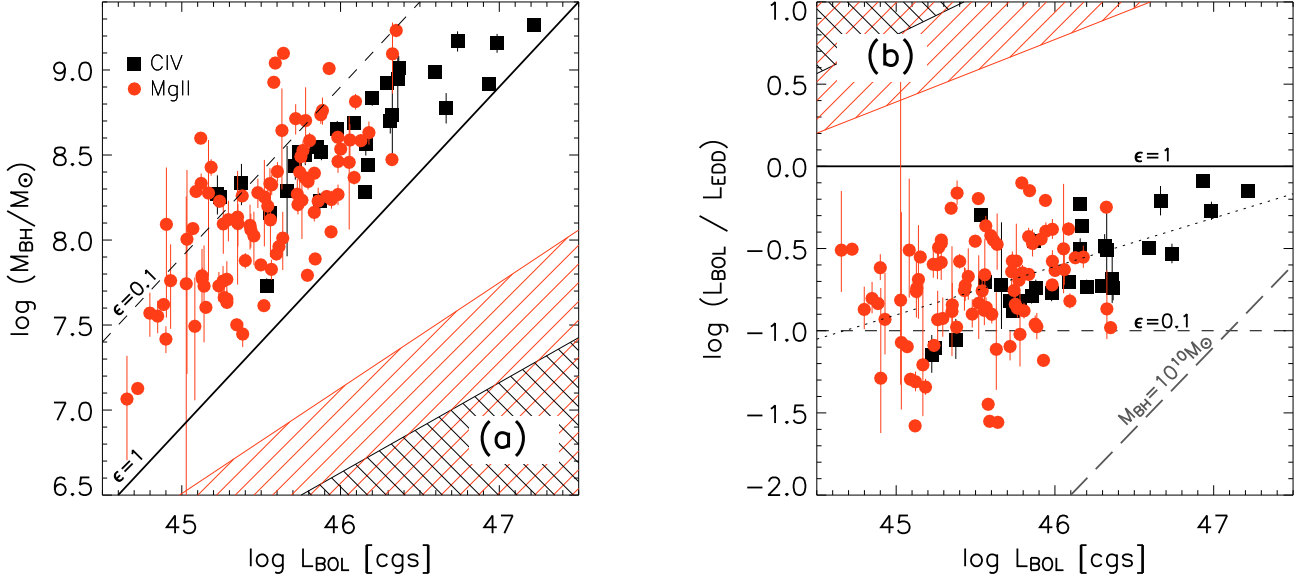


**Fig. 2.** Distribution of inferred BH masses (left) and Eddington ratios (right) versus AGN bolometric luminosities for the VVDS sample. The solid line and the dashed line correspond to Eddington ratios of  $\epsilon = 1$  and  $\epsilon = 0.1$ , respectively. Different symbols denote the emission line used for the mass estimate: red filled circles indicate that the black hole masses were derived from Mg II, while the black squares correspond to C IV. Error bars correspond to our uncertainties on the line width measurements. Inside the hashed regions, AGN would have emission lines with  $FWHM < 1000 \text{ km s}^{-1}$  implying that they would have been missed in our sample. The dotted line in panel b) shows a linear regression relation. (This figure is available in color in electronic form.)

size-luminosity exponent  $\gamma$ . However, also in this case, the correlation would have a smaller scatter for the C IV AGN than for the Mg II AGN.

We now consider possible sources of systematic errors, starting with sample incompleteness. Obviously, a selection bias against low mass black holes with high Eddington ratios would depopulate the lower left part of the left panel in Fig. 2, where AGN with high  $\epsilon$  would be located. AGN with low  $M_{\text{BH}}$  and high  $\epsilon$  are characterized by relatively narrow emission lines. As the VVDS AGN sample is defined through the detection of broad emission lines in low-resolution spectra, such a selection bias can in principle exist. However, from the spectral resolution of  $350 \text{ km s}^{-1}$  we expect the sample to be reasonably complete for lines intrinsically broader than  $\sim 1000 \text{ km s}^{-1}$ . This is shown in Fig. 2 where the areas of incompleteness corresponding to  $FWHM \leq 1000 \text{ km s}^{-1}$  are marked as hashed regions. It is clear that the lack of high  $\epsilon$  objects among the low luminosity AGN cannot predominantly be due to limited spectral resolution.

Since we are probing the AGN population down to low luminosities, host galaxy contamination could cause us to overestimate AGN continuum luminosities. This would lead to an overestimation of BH masses ( $M_{\text{BH}} \propto L^{\gamma}$ ) as well as Eddington ratios ( $\epsilon \propto L^{1-\gamma}$ ). We use here the result of the SED analysis presented in Bongiorno et al. (2007) to estimate the host galaxy contribution to the total continuum flux. The multi-wavelength coverage necessary for this analysis is available for about a fourth of the objects of our sample. Most of them (23/28) are in the low redshift range. Figure 3 is a version of Fig. 2b, corrected for this effect. We find that host contamination at  $1500 \text{ \AA}$  is negligible for all our objects. At  $3000 \text{ \AA}$ , this correction exceeds 0.1 dex in term of bolometric luminosities for 6 out of 23 AGN. These six objects are all in our “low luminosity” sample and therefore our conclusions are reinforced:  $\sim 30\%$  of the low luminosity AGN are likely to have somewhat smaller Eddington ratios than our above estimates.

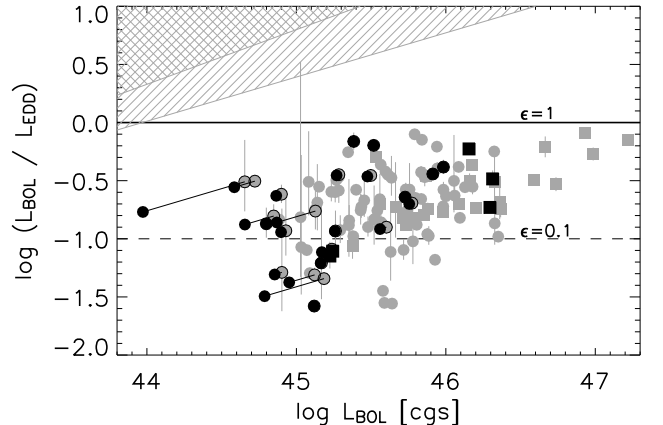


**Fig. 3.** Effect of host galaxy contamination on the distribution of AGN Eddington ratios versus bolometric luminosities. All points of Fig. 2 are reported in grey with the same symbol convention. Objects for which an estimate of their host galaxy contamination is available are shown with an open black symbol linked to a filled black symbol, corresponding to the position of these objects, respectively before and after correction.

Finally, we verified that the result presented here would have not been significantly different if we had included also the 16 low  $S/N$  objects.

## 5. Discussion

### 5.1. Comparison with other studies

Kollmeier et al. (2006) determined black hole masses for a sample of  $\sim 400$  AGN with optical magnitudes  $R \leq 21.5$ , in the context of the AGES survey. Their compilation shows a nearly constant Eddington ratio of  $\sim 0.25$ , with a dispersion of only  $\sim 0.3$  dex, over a wide range of luminosities and redshifts. Our

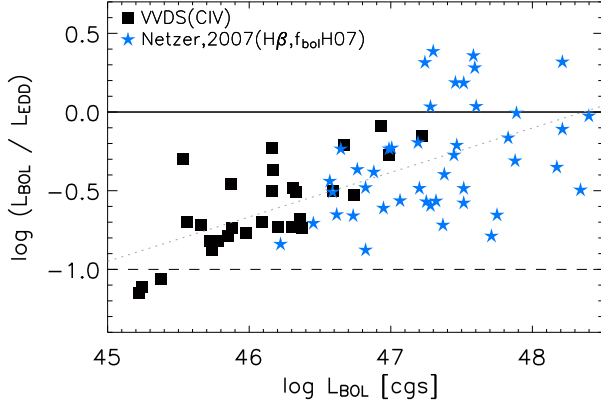


**Fig. 4.** Distribution of Eddington ratios versus bolometric luminosities of VVDS high redshift and Netzer et al. (2007) sample. For comparison purpose, Eddington ratios and bolometric luminosities of the latter sample have been recomputed with a luminosity dependent correction factor ( $9.6 < f_{\text{bol}}(5100 \text{ \AA}) < 10.5$ , Hopkins et al. 2007). The dotted line shows a linear regression relation ( $\log \epsilon \propto 0.29 \log L_{\text{bol}}$ ).

lower redshift sample overlaps with their Mg II virial masses in the luminosity range  $45 \lesssim \log L_{\text{bol}} \lesssim 46 \text{ erg s}^{-1}$ . If we superficially compare their results with ours in this range, we find them to be marginally inconsistent. The probability returned from a KS-test for the two samples to have their Eddington ratios drawn from the same distribution is  $P = 9\%$ . However, this difference is only caused by the different recipes used to estimate bolometric luminosities and, in particular, black hole masses. If we recompute the BH masses and bolometric luminosities of the Kollmeier et al. (2006) sample with the same recipes used in the present paper, we find that the two samples are fully consistent with each other.

In particular, Kollmeier et al. (2006) adopted a very steep exponent for the empirical luminosity-size relation for the Mg II emission line,  $\gamma = 0.88$  ( $R \propto L^\gamma$ ), whereas we employed  $\gamma = 0.62$  which is directly taken from the calibration by McLure & Dunlop (2004). A larger  $\gamma$  makes the  $L_{\text{bol}} - M_{\text{BH}}$  relation appear steeper and results in smaller  $M_{\text{BH}}$  and higher  $\epsilon$  values for the lower luminosity AGN.

However, we believe that there are good reasons against such a high value of  $\gamma$ . Recent reverberation mapping studies (Paltani & Türler 2005; Kaspi et al. 2007) suggest a rather flat luminosity-size relation also at high luminosities with  $\gamma$  even approaching 0.5 (corresponding to an approximately luminosity-independent ionization parameter in the broad-line region of AGN). A low value of  $\gamma \sim 0.5$  is also indicated for low redshift AGN after correction for host galaxy contributions (Bentz et al. 2006). Our adopted value of  $\gamma = 0.62$  may therefore even be considered conservative.

More recently, Netzer et al. (2007) also found a positive trend of  $\epsilon$  with luminosity for AGN with redshift 2.3–3.4.

They derived virial black hole masses from the redshifted H $\beta$  line observed in the near infrared, thus applying directly the reverberation mapping based calibration (although some extrapolation towards high luminosities was required).

Given the match in redshift range, we decided to combine the results by Netzer et al. with our C IV sample. The results are shown in Fig. 4 where, for consistency, we have recomputed the bolometric luminosities and Eddington ratios of the AGN in Netzer's sample using the same bolometric corrections we employed for our data, i.e. applying the Hopkins et al. (2007) luminosity-dependent SED model. The combined sample covers now more than three orders of magnitude in luminosity, with

most of our objects being much fainter than those in Netzer's sample. For the luminosity range common to both samples, the values of  $\epsilon$  are in very good agreement, despite the fact that we could only use the less trustworthy C IV lines.

Looking at the combined dataset there is again evidence of a correlation of Eddington ratios. In fact, the best-fit regression (dotted line in Fig. 4) returns  $\log \epsilon = -0.97 + 0.28 \log (L_{\text{bol}} - 45)$ , which is almost indistinguishable from the fit to only the combined VVDS Mg II + C IV sample. Thus the slow increase in Eddington ratios with bolometric luminosities seems to be a remarkably continuous property of high-redshift type 1 AGN, from the very low luminosities of the VVDS AGN to the highly luminous quasars in the sample of Netzer et al. (On the other hand, the dispersion of Eddington ratios in the Netzer sample is larger than in the VVDS, in particular due to the significant number of super-Eddington objects in the former.)

Very recently, Shen et al. (2008) employed a very large sample of SDSS quasar spectra to investigate systematic effects and biases in the derivation of relations between luminosities and black hole masses. They essentially confirm the low apparent dispersion in  $\epsilon$  of  $\lesssim 0.3$  found already by Kollmeier et al. (2006), however with the exception of their lowest luminosity (and also lowest redshift,  $z < 1$ ) bin where the dispersion increases to 0.42 dex. Thus, while there is essentially no overlap in the luminosity-redshift plane between SDSS and VVDS, the trends observed in our VVDS sample seems to be consistent with the SDSS results.

Babić et al. (2007) argue that an apparent trend of  $\epsilon$  as a function of luminosity is expected if one convolves a double power-law black hole mass function with a relatively broad distribution of Eddington ratios truncated at  $\epsilon = 1$ . We note however that the observed distribution of  $\epsilon$  is too symmetric and too narrow for this to be a strong effect: the apparent upper bound of  $\epsilon$  evolves along with  $L_{\text{bol}}$  from  $\log \epsilon < -0.5$  at  $\log L_{\text{bol}} \sim 45$  to  $\log \epsilon < 0.5$  for the high-luminosity objects in the sample by Netzer et al. (2007). In other words, there is no clear evidence of a physical truncation at a fixed  $\epsilon$ . It is of course still possible that AGN accretion physics imposes some unknown biases on the distribution of Eddington ratios, which may even depend on luminosity or black hole mass, in which case an effect such as described by Babić et al. (2007) may become relevant at some level. Much larger samples and a better understanding of the underlying physical processes would be required to investigate such effects.

## 5.2. Relation to the AGN luminosity function

At fixed redshift, the AGN luminosity function (AGNLF) is generally described as a double power-law. It has now become clear that its shape evolves with redshift, with a marked break for  $z > 1$  which almost disappears at lower redshift, as the faint-end slope steepens towards later cosmic times (e.g. Hasinger et al. 2005; Hopkins et al. 2007; Bongiorno et al. 2007). The luminous part of the AGNLF is dominated by black holes that appear to be typically accreting close to the Eddington limit ( $\epsilon \sim 0.1\text{--}1$ ), with relatively little dispersion, so that luminosities are roughly proportional to black hole masses, and this part of the AGNLF closely mirrors the black hole mass function.

The flat part of the AGNLF, on the other hand, could be composed of either low mass black holes also accreting close to Eddington, or of high-mass black holes with very low accretion rates, or of a mixture. In the context of a simple model where black hole growth and nuclear activity is triggered by galaxy mergers, Cattaneo (2001) first suggested that the faint

end slope of the AGNLF could be dominated by objects observed in the decaying phase of their light curve, well past their peak of activity. This idea was recently followed up by numerical simulations of galaxy mergers incorporating AGN feedback. For example Hopkins et al. (2006) find that the observed redshift evolution of the faint-end slope of the AGN luminosity function (flatter at higher redshift) is well reproduced with the luminosity-dependent quasar lifetime that they derive from extensive numerical simulation of galaxy mergers.

Our observations show that while some of the low-luminosity AGN in our sample have just low  $M_{\text{BH}}$ , many have instead the properties (i.e. high  $M_{\text{BH}}$ , low  $\epsilon$ ) predicted by these models. This is consistent with the suggested picture in which the faint end of the AGN luminosity function is populated with black holes that have exhausted a substantial fraction of their fuel. We speculate that at these redshifts we see glimpses of a population of AGN with black hole masses similar to those of luminous quasars, but already half starved and on their way to get extinguished.

From an analysis of a heterogeneous sample of low redshift AGN, Woo & Urry (2002) find that small Eddington ratios are found mainly for AGN with  $\log L_{\text{bol}} \leq 44.5$ , which in their sample are represented only by local Seyfert galaxies at  $z \leq 0.1$  (see their Fig. 8). Comparing their results with our measurements at  $z \gtrsim 1$  suggests that the luminosity below which such small Eddington ratios are found may evolve with redshift. This is, at least qualitatively, consistent with the observed redshift evolution of the break of the AGN luminosity function.

## 6. Conclusions

The VVDS is the first large spectroscopic AGN survey to probe luminosities as low as  $\log L_{\text{bol}} \lesssim 45$  at redshifts  $z > 1$ . We estimated black hole masses and Eddington ratios for 120 AGN. The main result of our study is a marked increase in the dispersion in Eddington ratios towards lower AGN bolometric luminosities. A substantial fraction of black holes in low- $L$  AGN accretes at less than 10% of their Eddington limits, whereas such low accretors are rare among AGN with higher  $L$ .

Our data also suggest that on average, the Eddington ratios systematically increase with nuclear luminosity. In the presence of substantial scatter and limited luminosity coverage, this trend is not easy to quantify; the slope of a relation  $\epsilon \propto L^\alpha$  depends on the adopted exponent in the empirical luminosity-size relation needed for virial scaling relations. Tentatively combining our data with those of Netzer et al. (2007), however, leads to

fully consistent results and underlines the indicated trend of  $\epsilon$  increasing with  $L_{\text{bol}}$ .

It is currently widely discussed how accurate the black hole masses and Eddington ratios based on single-epoch spectra can be. The best line is clearly H $\beta$  as here the luminosity-size relation has been directly calibrated with reverberation mapping. Mg II-based estimates can be cross-calibrated with H $\beta$  measurements and correlate quite well (McLure & Jarvis 2002; Shen et al. 2008). The C IV line, on the other hand, is under suspicion of representing gas that is not necessarily in or even close to virial equilibrium. One strong indication for such non-gravitational effects is the systematic blueshift of C IV with respect to low ionization lines (Gaskell 1982; Tytler & Fan 1992), which in combination with often asymmetric profiles (Richards et al. 2002) can be interpreted as the result of obscuration or radiative pressure. Consequently, the C IV emission line is often considered as not well suited to estimate black hole masses. Baskin & Laor (2005) and Netzer et al. (2007) found only a weak correlation between virial black hole mass estimates based on H $\beta$  and C IV. Similarly, Shen et al. (2008) noted a much tighter correlation between H $\beta$  and Mg II than between Mg II and C IV. For our VVDS sample, however, the observed trends between Mg II and C IV based subsamples (and also the H $\beta$  sample by Netzer et al. 2007) are highly consistent. In fact, the observed scatter in the  $L_{\text{bol}} - \epsilon$  relation is *lower* for the C IV objects than for the Mg II ones. It may be that radiation pressure and outflows are relevant in particular for high-luminosity QSOs (as has been also suggested by Marconi et al. 2008), and that therefore virial mass estimates based on C IV are more reliable for the faint AGN sampled in the VVDS than for other surveys.

While the “virial estimator” is likely to remain for some time the only practical method to obtain statistics on black hole masses at substantial redshifts, the present dependency of all measurements on the small number of low- $z$  reverberation-mapped AGN is unsatisfactory. It would be highly desirable if directly calibrated luminosity-size relations could be established also for higher redshifts and other lines than H $\beta$ .

*Acknowledgements.* We thank the referee, Marco Salvati, for his constructive comments that have led to improve this publication. We are grateful to Marianne Vestergaard for providing us with her UV Fe II templates, as well as to Juna Kollmeier and Hagai Netzer for communicating us the data table of their publications for our comparison purpose. We thank Suzy Collin and Asmus Böhm for helpful discussions.

## Appendix A: Mbh tables

**Table A.1.** Black hole masses and Eddington ratios estimated from the Mg II emission line.

Object ID (1)	$z$ (2)	$I_{\text{AB}}$ (3)	$S/N$ (4)	$\log \lambda L_{3000}$ (5)	$\log L_{\text{bol}}$ (6)	$FWHM$ (7)	$\log \frac{M_{\text{BH}}}{M_{\odot}}$ (8)	$\log \epsilon$ (9)
220551387	1.881	21.55	11.5	45.00	45.83	3277	8.16	-0.43
140265284	1.855	21.45	16.7	44.89	45.73	3730	8.21	-0.58
220082140	1.848	20.68	18.2	45.23	46.05	3903	8.46	-0.50
100113463	1.844	20.52	34.0	45.27	46.09	5720	8.81	-0.82
220090821	1.833	20.49	15.5	45.26	46.09	3442	8.37	-0.38
140520998	1.829	20.89	26.5	45.06	45.89	6286	8.76	-0.98
140363408	1.826	21.87	11.3	44.97	45.81	5448	8.58	-0.88
100110223	1.826	21.35	7.9	44.92	45.76	3770	8.23	-0.58
140495178	1.824	20.80	29.6	45.24	46.06	4525	8.59	-0.63
020461459	1.821	21.60	20.8	44.89	45.73	4016	8.27	-0.64
220308643	1.801	21.89	11.2	44.79	45.63	6649	8.64	-1.11

**Table A.1.** continued.

Object ID	$z$	$I_{AB}$	$S/N$	$\log \lambda L_{3000}$	$\log L_{\text{bol}}$	$FWHM$	$\log \frac{M_{\text{BH}}}{M_{\odot}}$	$\log \epsilon$
(1)	(2)	(3)	(4)	(5)	(6)	(7)	(8)	(9)
100122852	1.801	19.90	54.1	45.52	46.33	6649	9.09	-0.87
100507363	1.784	21.69	14.1	44.79	45.64	3195	8.01	-0.47
100451895	1.781	20.08	28.9	45.51	46.32	3257	8.47	-0.25
220438495	1.774	21.93	10.7	44.67	45.52	4606	8.25	-0.83
100232259	1.765	21.13	10.2	44.88	45.72	6749	8.71	-1.10
140433507	1.765	21.13	13.2	44.95	45.78	6356	8.70	-1.02
020278210	1.757	21.36	26.4	44.76	45.60	5144	8.40	-0.90
020254511	1.747	20.66	49.8	45.08	45.91	3442	8.26	-0.44
220370320	1.745	20.22	25.2	45.36	46.18	4352	8.63	-0.55
220409734	1.742	21.90	10.2	44.77	45.61	3071	7.96	-0.45
220159199	1.722	22.12	9.1	44.58	45.43	4067	8.09	-0.76
020177875	1.682	22.53	8.0	44.32	45.18	7263	8.43	-1.34
220427244	1.681	20.40	16.5	45.31	46.13	4281	8.58	-0.56
220371301	1.645	22.18	12.2	44.72	45.57	4830	8.32	-0.86
020232397	1.628	22.69	11.2	44.25	45.13	3637	7.79	-0.76
000033629	1.621	22.14	14.7	44.50	45.35	4362	8.10	-0.84
020114448	1.614	22.24	8.5	44.37	45.24	5539	8.23	-1.09
020120394	1.612	20.38	64.6	45.16	45.98	3308	8.27	-0.38
020466135	1.581	21.13	63.6	44.94	45.77	4342	8.37	-0.69
020147295	1.556	22.59	14.0	44.30	45.17	6175	8.28	-1.21
100290682	1.549	21.49	17.7	44.75	45.60	2957	7.92	-0.42
220566905	1.528	22.38	13.9	44.49	45.35	2211	7.50	-0.25
020210524	1.515	20.41	82.2	45.18	46.00	4444	8.53	-0.63
220610034	1.513	20.66	42.3	45.12	45.94	3298	8.24	-0.39
020176565	1.504	23.24	11.5	44.01	44.90	2822	7.42	-0.62
220327763	1.501	21.36	36.2	44.96	45.80	4159	8.34	-0.65
220568559	1.498	22.21	12.3	44.49	45.35	4566	8.13	-0.88
220609820	1.479	21.64	18.9	44.71	45.56	3832	8.12	-0.66
220419246	1.479	20.73	20.2	45.05	45.88	6155	8.74	-0.96
220376198	1.469	21.75	18.5	44.63	45.48	4891	8.28	-0.90
220377744	1.465	21.18	15.4	44.80	45.64	11129	9.10	-1.56
100046262	1.463	20.96	39.1	44.93	45.76	5255	8.53	-0.86
220469918	1.460	21.89	11.2	44.40	45.27	2822	7.66	-0.49
140338689	1.442	20.74	37.6	44.96	45.79	2211	7.79	-0.10
140441955	1.429	22.06	16.6	44.58	45.43	3934	8.06	-0.73
020367106	1.397	22.42	10.7	44.19	45.07	5235	8.07	-1.10
220326578	1.391	22.23	11.6	44.28	45.15	2884	7.60	-0.55
020463196	1.388	23.27	8.5	43.74	44.65	2275	7.06	-0.51
020179225	1.386	22.39	28.5	44.25	45.12	9293	8.60	-1.58
140305471	1.370	21.08	16.5	44.69	45.54	4261	8.20	-0.76
220554600	1.369	20.78	27.6	44.91	45.74	4606	8.40	-0.76
020467628	1.358	21.35	30.7	44.65	45.50	2957	7.85	-0.46
020258622	1.339	22.74	16.1	44.04	44.93	4097	7.76	-0.93
100198426	1.337	22.14	9.5	44.15	45.03	3719	7.74	-0.81
220093875	1.337	21.94	10.0	44.37	45.23	3133	7.73	-0.60
020165108	1.322	23.09	9.6	43.82	44.72	2317	7.13	-0.50
020163018	1.321	23.11	13.3	43.95	44.85	3432	7.55	-0.80
220542377	1.310	21.24	24.5	44.73	45.58	9574	8.93	-1.45
140222324	1.305	21.72	20.0	44.42	45.28	2759	7.65	-0.47
220525793	1.294	19.13	98.3	45.54	46.35	7655	9.23	-0.98
220247296	1.285	21.52	22.2	44.52	45.38	5154	8.26	-0.98
020118483	1.261	22.86	12.0	43.90	44.80	3637	7.57	-0.87
000028880	1.257	22.71	18.5	43.99	44.89	3607	7.62	-0.83
220613346	1.253	20.51	37.4	45.00	45.84	4271	8.39	-0.66
100139500	1.248	21.01	20.1	44.71	45.56	4911	8.33	-0.88
020213000	1.225	21.44	20.7	44.40	45.26	4667	8.09	-0.93
220081925	1.217	21.79	11.9	44.42	45.28	3154	7.77	-0.58
020237445	1.214	22.43	8.0	44.01	44.90	6124	8.09	-1.29
220375302	1.208	21.82	13.1	44.43	45.29	4688	8.12	-0.93
140433055	1.208	22.33	27.0	44.27	45.14	3360	7.73	-0.69

**Table A.1.** continued.

Object ID	$z$	$I_{AB}$	$S/N$	$\log \lambda L_{3000}$	$\log L_{bol}$	$FWHM$	$\log \frac{M_{BH}}{M_\odot}$	$\log \epsilon$
(1)	(2)	(3)	(4)	(5)	(6)	(7)	(8)	(9)
100048462	1.203	20.48	42.5	44.91	45.75	5093	8.49	-0.84
220255701	1.193	19.77	63.9	45.11	45.94	2655	8.05	-0.21
020086859	1.192	20.97	27.7	44.67	45.52	2211	7.61	-0.20
140306523	1.190	20.10	60.6	45.16	45.98	4880	8.60	-0.72
100210521	1.172	21.63	18.8	44.40	45.26	3174	7.76	-0.60
220567825	1.160	21.19	23.8	44.72	45.56	2728	7.83	-0.36
100338914	1.158	19.78	57.2	45.16	45.98	4138	8.46	-0.58
020364478	1.157	21.74	25.5	44.25	45.12	6830	8.33	-1.31
140192158	1.127	22.12	17.1	44.15	45.03	5012	8.00	-1.07
220561414	1.124	20.11	49.8	45.01	45.84	2381	7.89	-0.15
220357650	1.123	22.34	14.2	44.21	45.08	2675	7.49	-0.51
020243922	1.120	21.29	44.8	44.42	45.28	2696	7.63	-0.45
140443623	1.120	21.48	16.7	44.26	45.13	3555	7.77	-0.74
100241696	1.111	22.00	11.3	44.21	45.09	6628	8.29	-1.30
220458211	1.105	20.69	36.8	45.03	45.86	3473	8.23	-0.47
220463317	1.066	19.62	43.8	45.10	45.93	8098	9.01	-1.18
020329650	1.050	20.84	36.0	44.53	45.38	2018	7.45	-0.16
140278593	1.046	20.50	36.7	44.74	45.59	10828	9.04	-1.55
220152300	1.038	20.69	19.2	44.54	45.40	3277	7.88	-0.58
220586430	1.028	20.45	26.8	44.60	45.45	3719	8.02	-0.67

Table columns: (1) Object identification number of the VVDS database. (2) Redshift. (3)  $I$  magnitudes in the AB system. (4) Mean  $S/N$  per pixel in the vicinity of the broad-emission line. (5) Monochromatic luminosity at 3000 Å in erg s $^{-1}$ . (6) Corresponding bolometric luminosity in erg s $^{-1}$ . (7)  $FWHM$  of the Mg II in km s $^{-1}$ . (8) Estimate of the virial black hole Mass as obtained from Eq. (1). (9) Eddington ratio.

**Table A.2.** Black hole masses and Eddington ratios estimated from the C IV emission line.

Object ID	$z$	$I_{AB}$	$S/N$	$\log \lambda L_{1350}$	$\log L_{bol}$	$\sigma$	$\log \frac{M_{BH}}{M_\odot}$	$\log \epsilon$
(1)	(2)	(3)	(4)	(5)	(6)	(7)	(8)	(9)
220183694	4.193	20.27	33.1	46.34	46.93	2976	8.92	-0.09
020254576	3.853	21.15	35.5	45.71	46.31	3406	8.70	-0.48
220267678	3.833	21.44	11.9	45.72	46.33	3534	8.74	-0.51
020277536	3.626	23.55	16.7	44.58	45.24	4032	8.25	-1.11
220055529	3.594	21.52	9.6	45.76	46.37	4708	9.01	-0.74
100471137	3.494	20.12	39.6	46.07	46.67	2994	8.78	-0.21
020179116	3.308	23.89	10.4	44.56	45.22	4191	8.27	-1.15
140465826	3.290	20.16	60.3	46.14	46.74	4486	9.17	-0.53
020465339	3.285	21.09	65.2	45.69	46.30	4476	8.93	-0.73
100049642	3.192	20.55	41.7	45.75	46.36	4385	8.94	-0.68
140191403	3.170	22.15	19.1	45.36	45.98	3988	8.65	-0.77
220359141	3.158	22.64	10.5	44.72	45.38	4079	8.33	-1.06
220157547	3.152	22.26	8.1	45.03	45.66	3211	8.29	-0.72
220133794	3.147	22.29	17.9	45.24	45.87	2623	8.23	-0.46
220617869	3.133	22.36	12.8	45.08	45.72	3673	8.43	-0.82
220309346	3.090	22.22	21.8	45.10	45.74	3987	8.52	-0.88
220391155	3.087	21.07	31.5	45.56	46.17	2759	8.44	-0.37
100245809	3.079	21.67	19.1	45.25	45.88	3650	8.52	-0.74
220205172	3.076	19.17	83.7	46.40	46.99	3789	9.16	-0.27
220133609	3.051	20.40	39.7	45.99	46.59	3994	8.99	-0.50
220056847	3.001	21.47	26.4	45.59	46.20	4275	8.83	-0.73
220044408	2.910	21.28	17.4	45.15	45.78	3806	8.50	-0.82
140493205	2.865	21.66	24.2	45.23	45.85	3821	8.54	-0.79
220181962	2.856	18.72	125.1	46.64	47.22	3706	9.26	-0.15
140040016	2.838	21.55	39.8	45.47	46.09	3896	8.69	-0.70
140432542	2.800	21.85	17.2	45.55	46.16	3210	8.56	-0.50
020268754	2.719	20.59	63.0	45.54	46.16	2332	8.28	-0.23
100168207	2.715	22.46	24.4	44.89	45.53	1840	7.73	-0.30
220001963	2.680	22.28	13.5	44.92	45.56	2968	8.16	-0.70

Table columns: (1) Object identification number of the VVDS database. (2) Redshift. (3)  $I$  magnitudes in the AB system. (4) Mean  $S/N$  per pixel in the vicinity of the broad-emission line. (5) Monochromatic luminosity at 1350 Å in erg s $^{-1}$ . (6) Corresponding bolometric luminosity in erg s $^{-1}$ . (7) Emission line velocity dispersion,  $\sigma$  of the C IV in km s $^{-1}$ . (8) Estimate of the virial black hole Mass as obtained from Eq. (2). (9) Eddington ratio.

## Appendix B: Catalog of VVDS broad-line AGN (first and second-epoch data)

**Table B.1.** Catalog of broad-line AGN with secure redshift.

Object ID (1)	$\alpha_{J2000}$ (2)	$\delta_{J2000}$ (3)	$z$ (4)	Flag (5)	Epoch (6)	$B_{AB}$ (7)	$V_{AB}$ (8)	$R_{AB}$ (9)	$I_{AB}$ (10)	Morphology (11)	Remark (12)
<b>CDFS:</b>											
000018607	03 <sup>h</sup> 32 <sup>m</sup> 18.26 <sup>s</sup>	-27 <sup>°</sup> 52 <sup>m</sup> 41.42 <sup>s</sup>	2.8010	14	1	23.94	24.62	24.08	23.91	...	...
000025363	03 <sup>h</sup> 32 <sup>m</sup> 59.85 <sup>s</sup>	-27 <sup>°</sup> 47 <sup>m</sup> 48.42 <sup>s</sup>	2.5673	14	1	22.09	21.66	21.92	21.95	...	...
000023526	03 <sup>h</sup> 32 <sup>m</sup> 43.25 <sup>s</sup>	-27 <sup>°</sup> 49 <sup>m</sup> 14.38 <sup>s</sup>	1.9199	14	1	22.53	22.70	22.65	22.17	...	Sz.
000033629	03 <sup>h</sup> 32 <sup>m</sup> 25.17 <sup>s</sup>	-27 <sup>°</sup> 42 <sup>m</sup> 19.05 <sup>s</sup>	1.6207	14	1	24.33	23.90	22.94	22.14	...	...
000073509	03 <sup>h</sup> 32 <sup>m</sup> 02.47 <sup>s</sup>	-27 <sup>°</sup> 46 <sup>m</sup> 00.53 <sup>s</sup>	1.6199	14	1	25.34	24.59	23.95	23.62	...	Sz.
000028880	03 <sup>h</sup> 33 <sup>m</sup> 03.62 <sup>s</sup>	-27 <sup>°</sup> 45 <sup>m</sup> 18.97 <sup>s</sup>	1.2574	14	1	23.78	23.30	22.98	22.71	...	Sz.
000031947	03 <sup>h</sup> 32 <sup>m</sup> 00.37 <sup>s</sup>	-27 <sup>°</sup> 43 <sup>m</sup> 19.85 <sup>s</sup>	1.0401	14	1	22.99	22.25	22.13	22.12	...	Sz.
000037399	03 <sup>h</sup> 32 <sup>m</sup> 38.14 <sup>s</sup>	-27 <sup>°</sup> 39 <sup>m</sup> 45.02 <sup>s</sup>	0.8366	14	1	20.84	20.43	20.41	20.44	...	...
000029274	03 <sup>h</sup> 32 <sup>m</sup> 30.23 <sup>s</sup>	-27 <sup>°</sup> 45 <sup>m</sup> 04.75 <sup>s</sup>	0.7352	14	1	22.67	22.30	22.05	21.62	...	...
000037103	03 <sup>h</sup> 32 <sup>m</sup> 37.47 <sup>s</sup>	-27 <sup>°</sup> 40 <sup>m</sup> 00.33 <sup>s</sup>	0.6656	14	1	23.11	22.93	22.46	21.84	...	...
0226-04	Deep mode	58 AGN									
020254576	02 <sup>h</sup> 25 <sup>m</sup> 27.23 <sup>s</sup>	-04 <sup>°</sup> 26 <sup>m</sup> 31.02 <sup>s</sup>	3.8527	14	1	23.35	21.80	21.46	21.15	point-like	...
020277536	02 <sup>h</sup> 27 <sup>m</sup> 53.85 <sup>s</sup>	-04 <sup>°</sup> 23 <sup>m</sup> 20.10 <sup>s</sup>	3.6260	14	1	25.26	23.89	23.61	23.56	...	...
020169816	02 <sup>h</sup> 25 <sup>m</sup> 45.04 <sup>s</sup>	-04 <sup>°</sup> 37 <sup>m</sup> 35.95 <sup>s</sup>	3.5893	14	1	24.67	22.96	22.65	22.15	point-like	FORS
020351846	02 <sup>h</sup> 26 <sup>m</sup> 30.84 <sup>s</sup>	-04 <sup>°</sup> 13 <sup>m</sup> 26.09 <sup>s</sup>	3.5680	14	1	25.06	23.71	23.24	22.80	...	FORS
020467962	02 <sup>h</sup> 26 <sup>m</sup> 59.17 <sup>s</sup>	-04 <sup>°</sup> 16 <sup>m</sup> 55.89 <sup>s</sup>	3.3247	13	1	25.23	23.97	23.80	23.59	...	...
020179116	02 <sup>h</sup> 25 <sup>m</sup> 34.98 <sup>s</sup>	-04 <sup>°</sup> 36 <sup>m</sup> 16.46 <sup>s</sup>	3.3080	14	1	25.19	23.95	23.85	23.90	...	FORS
020118986	02 <sup>h</sup> 26 <sup>m</sup> 54.53 <sup>s</sup>	-04 <sup>°</sup> 44 <sup>m</sup> 37.72 <sup>s</sup>	3.3018	14	1	25.43	23.99	23.98	23.58	...	...
020465339	02 <sup>h</sup> 27 <sup>m</sup> 06.44 <sup>s</sup>	-04 <sup>°</sup> 19 <sup>m</sup> 24.30 <sup>s</sup>	3.2852	14	1	21.78	21.32	21.00	21.10	point-like	...
020461765	02 <sup>h</sup> 26 <sup>m</sup> 35.95 <sup>s</sup>	-04 <sup>°</sup> 23 <sup>m</sup> 21.81 <sup>s</sup>	3.2831	14	1	24.62	23.01	22.87	22.89	...	...
020180665	02 <sup>h</sup> 26 <sup>m</sup> 45.46 <sup>s</sup>	-04 <sup>°</sup> 36 <sup>m</sup> 15.43 <sup>s</sup>	3.2619	14	1	21.09	19.32	19.03	18.15	point-like	...
020164607	02 <sup>h</sup> 25 <sup>m</sup> 32.46 <sup>s</sup>	-04 <sup>°</sup> 38 <sup>m</sup> 18.63 <sup>s</sup>	2.9220	14	1	23.93	23.46	23.21	23.11	...	...
020205812	02 <sup>h</sup> 27 <sup>m</sup> 23.84 <sup>s</sup>	-04 <sup>°</sup> 32 <sup>m</sup> 31.69 <sup>s</sup>	2.8922	14	1	24.77	24.37	24.52	23.87	...	...
020131908	02 <sup>h</sup> 26 <sup>m</sup> 51.04 <sup>s</sup>	-04 <sup>°</sup> 42 <sup>m</sup> 56.55 <sup>s</sup>	2.7813	14	1	23.09	22.76	22.77	22.34	extended	...
020200020	02 <sup>h</sup> 25 <sup>m</sup> 50.40 <sup>s</sup>	-04 <sup>°</sup> 33 <sup>m</sup> 24.00 <sup>s</sup>	2.7373	13	1	21.96	22.10	21.73	21.92	point-like	...
020465540	02 <sup>h</sup> 26 <sup>m</sup> 44.48 <sup>s</sup>	-04 <sup>°</sup> 19 <sup>m</sup> 16.76 <sup>s</sup>	2.7372	14	1	24.15	23.95	23.82	23.58	...	...
020268754	02 <sup>h</sup> 26 <sup>m</sup> 09.63 <sup>s</sup>	-04 <sup>°</sup> 24 <sup>m</sup> 37.74 <sup>s</sup>	2.7187	14	1	20.57	20.60	20.76	20.59	point-like	...
020272573	02 <sup>h</sup> 26 <sup>m</sup> 26.13 <sup>s</sup>	-04 <sup>°</sup> 24 <sup>m</sup> 03.19 <sup>s</sup>	2.6823	14	1	24.30	23.93	23.59	23.63	...	...
020195823	02 <sup>h</sup> 27 <sup>m</sup> 24.10 <sup>s</sup>	-04 <sup>°</sup> 33 <sup>m</sup> 55.72 <sup>s</sup>	2.4250	14	1	24.20	23.62	23.85	23.38	...	FORS
020239945	02 <sup>h</sup> 27 <sup>m</sup> 31.14 <sup>s</sup>	-04 <sup>°</sup> 28 <sup>m</sup> 22.83 <sup>s</sup>	2.4247	14	1	23.66	23.13	23.14	22.90	...	FORS
020208084	02 <sup>h</sup> 27 <sup>m</sup> 29.24 <sup>s</sup>	-04 <sup>°</sup> 32 <sup>m</sup> 27.51 <sup>s</sup>	2.2850	214	1	19.34	19.10	19.12	19.04	point-like	FORS
020302785	02 <sup>h</sup> 26 <sup>m</sup> 24.63 <sup>s</sup>	-04 <sup>°</sup> 20 <sup>m</sup> 02.14 <sup>s</sup>	2.2357	14	1	21.43	21.27	21.35	21.01	point-like	...
020218399	02 <sup>h</sup> 27 <sup>m</sup> 31.34 <sup>s</sup>	-04 <sup>°</sup> 30 <sup>m</sup> 50.26 <sup>s</sup>	2.2255	14	1	22.92	22.40	22.54	22.19	point-like	FORS
020212038	02 <sup>h</sup> 26 <sup>m</sup> 08.40 <sup>s</sup>	-04 <sup>°</sup> 31 <sup>m</sup> 43.15 <sup>s</sup>	2.2082	14	1	22.91	22.28	22.02	21.46	extended	FORS
020234610	02 <sup>h</sup> 26 <sup>m</sup> 58.99 <sup>s</sup>	-04 <sup>°</sup> 29 <sup>m</sup> 06.02 <sup>s</sup>	2.1645	13	1	26.05	25.11	24.74	23.87	...	...
020188089	02 <sup>h</sup> 25 <sup>m</sup> 25.68 <sup>s</sup>	-04 <sup>°</sup> 35 <sup>m</sup> 09.45 <sup>s</sup>	2.1384	14	1	21.13	20.96	20.96	20.66	point-like	...
020342478	02 <sup>h</sup> 27 <sup>m</sup> 24.52 <sup>s</sup>	-04 <sup>°</sup> 14 <sup>m</sup> 40.01 <sup>s</sup>	2.0464	14	1	24.99	24.85	24.53	23.90	...	...
020286836	02 <sup>h</sup> 26 <sup>m</sup> 22.17 <sup>s</sup>	-04 <sup>°</sup> 22 <sup>m</sup> 21.62 <sup>s</sup>	2.0060	14	1	19.29	19.12	19.06	18.51	point-like	...
020291309	02 <sup>h</sup> 26 <sup>m</sup> 31.23 <sup>s</sup>	-04 <sup>°</sup> 21 <sup>m</sup> 28.87 <sup>s</sup>	1.9930	14	1	23.96	23.57	23.82	22.89	...	...
020159510	02 <sup>h</sup> 27 <sup>m</sup> 09.85 <sup>s</sup>	-04 <sup>°</sup> 39 <sup>m</sup> 02.21 <sup>s</sup>	1.9309	14	1	22.73	22.41	22.45	21.98	point-like	...
020461459	02 <sup>h</sup> 27 <sup>m</sup> 04.25 <sup>s</sup>	-04 <sup>°</sup> 23 <sup>m</sup> 37.77 <sup>s</sup>	1.8211	13	1	23.50	22.93	22.42	21.60	point-like	...
020278210	02 <sup>h</sup> 27 <sup>m</sup> 40.00 <sup>s</sup>	-04 <sup>°</sup> 23 <sup>m</sup> 17.43 <sup>s</sup>	1.7574	13	1	22.69	21.88	22.29	21.37	point-like	...
020254511	02 <sup>h</sup> 27 <sup>m</sup> 36.93 <sup>s</sup>	-04 <sup>°</sup> 26 <sup>m</sup> 31.30 <sup>s</sup>	1.7466	14	1	20.77	20.85	20.86	20.66	point-like	...
020177875	02 <sup>h</sup> 26 <sup>m</sup> 53.87 <sup>s</sup>	-04 <sup>°</sup> 36 <sup>m</sup> 27.21 <sup>s</sup>	1.6821	13	1	24.02	23.66	23.37	22.54	...	...
020232397	02 <sup>h</sup> 26 <sup>m</sup> 26.04 <sup>s</sup>	-04 <sup>°</sup> 29 <sup>m</sup> 27.88 <sup>s</sup>	1.6280	14	1	23.72	23.32	23.15	22.69	...	FORS
020114448	02 <sup>h</sup> 27 <sup>m</sup> 00.99 <sup>s</sup>	-04 <sup>°</sup> 45 <sup>m</sup> 16.83 <sup>s</sup>	1.6140	13	1	23.40	23.36	22.98	22.24	point-like	...
020120394	02 <sup>h</sup> 26 <sup>m</sup> 59.92 <sup>s</sup>	-04 <sup>°</sup> 44 <sup>m</sup> 30.32 <sup>s</sup>	1.6120	14	1	21.27	20.97	20.78	20.38	point-like	...
020466135	02 <sup>h</sup> 26 <sup>m</sup> 46.99 <sup>s</sup>	-04 <sup>°</sup> 18 <sup>m</sup> 37.56 <sup>s</sup>	1.5806	14	1	21.30	21.57	21.06	21.14	point-like	VIMOS
020147295	02 <sup>h</sup> 25 <sup>m</sup> 29.19 <sup>s</sup>	-04 <sup>°</sup> 40 <sup>m</sup> 44.16 <sup>s</sup>	1.5562	14	1	23.87	23.44	22.85	22.59	...	FORS
020210524	02 <sup>h</sup> 27 <sup>m</sup> 07.55 <sup>s</sup>	-04 <sup>°</sup> 32 <sup>m</sup> 02.98 <sup>s</sup>	1.5150	14	1	21.03	20.90	20.64	20.41	point-like	FORS
020176565	02 <sup>h</sup> 25 <sup>m</sup> 28.06 <sup>s</sup>	-04 <sup>°</sup> 36 <sup>m</sup> 41.59 <sup>s</sup>	1.5039	14	1	23.63	23.62	23.27	23.24	...	FORS
020223153	02 <sup>h</sup> 26 <sup>m</sup> 17.52 <sup>s</sup>	-04 <sup>°</sup> 30 <sup>m</sup> 29.27 <sup>s</sup>	1.4777	214	1	21.19	21.05	20.94	20.66	point-like	FORS
020367106	02 <sup>h</sup> 26 <sup>m</sup> 34.71 <sup>s</sup>	-04 <sup>°</sup> 11 <sup>m</sup> 33.98 <sup>s</sup>	1.3973	14	1	23.27	23.02	22.55	22.42	extended	FORS
020463196	02 <sup>h</sup> 27 <sup>m</sup> 00.65 <sup>s</sup>	-04 <sup>°</sup> 21 <sup>m</sup> 49.00 <sup>s</sup>	1.3875	14	1	24.50	24.43	23.92	23.28	...	...
020179225	02 <sup>h</sup> 27 <sup>m</sup> 02.15 <sup>s</sup>	-04 <sup>°</sup> 36 <sup>m</sup> 15.96 <sup>s</sup>	1.3860	13	1	23.91	23.51	23.02	22.39	point-like	...
020467628	02 <sup>h</sup> 27 <sup>m</sup> 04.06 <sup>s</sup>	-04 <sup>°</sup> 17 <sup>m</sup> 09.77 <sup>s</sup>	1.3582	13	1	21.98	21.82	21.62	21.36	point-like	...

**Table B.1.** continued.

Object ID (1)	$\alpha_{J2000}$ (2)	$\delta_{J2000}$ (3)	$z$ (4)	Flag (5)	Epoch (6)	$B_{AB}$ (7)	$V_{AB}$ (8)	$R_{AB}$ (9)	$I_{AB}$ (10)	Morphology (11)	Remark (12)
020258622	02 <sup>h</sup> 26 <sup>m</sup> 20.06 <sup>s</sup>	-04 <sup>°</sup> 25 <sup>m</sup> 54.51 <sup>s</sup>	1.3386	14	1	24.45	23.85	23.47	22.74	...	...
020165108	02 <sup>h</sup> 26 <sup>m</sup> 59.85 <sup>s</sup>	-04 <sup>°</sup> 38 <sup>m</sup> 12.68 <sup>s</sup>	1.3219	13	1	24.71	24.05	23.79	23.09	...	...
020163018	02 <sup>h</sup> 26 <sup>m</sup> 45.20 <sup>s</sup>	-04 <sup>°</sup> 38 <sup>m</sup> 30.58 <sup>s</sup>	1.3208	14	1	23.89	23.62	23.30	23.12	...	FORS
020118483	02 <sup>h</sup> 27 <sup>m</sup> 36.06 <sup>s</sup>	-04 <sup>°</sup> 44 <sup>m</sup> 41.89 <sup>s</sup>	1.2606	13	1	23.81	23.44	23.29	22.86	...	...
020213000	02 <sup>h</sup> 26 <sup>m</sup> 47.88 <sup>s</sup>	-04 <sup>°</sup> 31 <sup>m</sup> 35.20 <sup>s</sup>	1.2250	13	1	22.30	22.02	21.76	21.44	point-like	...
020237445	02 <sup>h</sup> 25 <sup>m</sup> 57.38 <sup>s</sup>	-04 <sup>°</sup> 28 <sup>m</sup> 46.04 <sup>s</sup>	1.2138	14	1	23.93	23.54	23.06	22.43	extended	...
020086859	02 <sup>h</sup> 26 <sup>m</sup> 29.62 <sup>s</sup>	-04 <sup>°</sup> 49 <sup>m</sup> 14.41 <sup>s</sup>	1.1921	13	1	22.99	21.98	21.44	20.97	point-like	...
020364478	02 <sup>h</sup> 26 <sup>m</sup> 49.41 <sup>s</sup>	-04 <sup>°</sup> 11 <sup>m</sup> 53.30 <sup>s</sup>	1.1573	14	1	22.94	22.74	22.25	21.74	extended	...
020243922	02 <sup>h</sup> 27 <sup>m</sup> 47.33 <sup>s</sup>	-04 <sup>°</sup> 27 <sup>m</sup> 53.20 <sup>s</sup>	1.1203	14	1	22.03	21.72	21.60	21.29	point-like	...
020329650	02 <sup>h</sup> 26 <sup>m</sup> 08.71 <sup>s</sup>	-04 <sup>°</sup> 16 <sup>m</sup> 34.53 <sup>s</sup>	1.0498	14	1	21.53	21.15	20.97	20.85	point-like	...
020158952	02 <sup>h</sup> 26 <sup>m</sup> 17.81 <sup>s</sup>	-04 <sup>°</sup> 39 <sup>m</sup> 08.50 <sup>s</sup>	0.8738	14	1	22.82	22.16	22.00	21.41	extended	...
020351277	02 <sup>h</sup> 25 <sup>m</sup> 57.41 <sup>s</sup>	-04 <sup>°</sup> 13 <sup>m</sup> 39.43 <sup>s</sup>	0.6061	14	1	20.61	20.40	20.32	19.84	extended	...
020190479	02 <sup>h</sup> 25 <sup>m</sup> 45.55 <sup>s</sup>	-04 <sup>°</sup> 34 <sup>m</sup> 45.18 <sup>s</sup>	0.1524	14	1	21.99	21.56	21.65	21.33	point-like	...
1003+01	Wide mode	34 AGN									
100481003	10 <sup>h</sup> 04 <sup>m</sup> 38.83 <sup>s</sup>	+02 <sup>°</sup> 12 <sup>m</sup> 33.88 <sup>s</sup>	5.0065	14	2	18.35	19.37	19.46	18.34	extended	...
100561715	10 <sup>h</sup> 04 <sup>m</sup> 26.84 <sup>s</sup>	+02 <sup>°</sup> 24 <sup>m</sup> 44.82 <sup>s</sup>	4.3600	14	2	...	23.47	22.67	21.89	point-like	...
100359356	10 <sup>h</sup> 03 <sup>m</sup> 38.72 <sup>s</sup>	+01 <sup>°</sup> 56 <sup>m</sup> 41.61 <sup>s</sup>	3.6805	14	2	22.93	21.39	21.45	20.75	point-like	...
100105943	10 <sup>h</sup> 03 <sup>m</sup> 46.33 <sup>s</sup>	+01 <sup>°</sup> 19 <sup>m</sup> 11.04 <sup>s</sup>	3.5553	13	1	...	...	...	21.15	point-like	...
100471137	10 <sup>h</sup> 02 <sup>m</sup> 56.58 <sup>s</sup>	+02 <sup>°</sup> 11 <sup>m</sup> 58.78 <sup>s</sup>	3.4938	14	2	21.51	20.46	20.46	20.08	point-like	...
100049642	10 <sup>h</sup> 03 <sup>m</sup> 42.42 <sup>s</sup>	+01 <sup>°</sup> 07 <sup>m</sup> 55.37 <sup>s</sup>	3.1918	13	2	...	...	...	20.51	point-like	...
100245809	10 <sup>h</sup> 04 <sup>m</sup> 00.36 <sup>s</sup>	+01 <sup>°</sup> 40 <sup>m</sup> 45.74 <sup>s</sup>	3.0789	14	1	22.71	22.01	21.94	21.62	point-like	...
100049420	10 <sup>h</sup> 07 <sup>m</sup> 13.20 <sup>s</sup>	+01 <sup>°</sup> 07 <sup>m</sup> 53.62 <sup>s</sup>	2.9450	14	2	...	...	...	21.57	point-like	...
100168207	10 <sup>h</sup> 04 <sup>m</sup> 36.55 <sup>s</sup>	+01 <sup>°</sup> 30 <sup>m</sup> 05.86 <sup>s</sup>	2.7152	14	1	22.38	21.84	22.14	22.40	point-like	...
100343840	10 <sup>h</sup> 04 <sup>m</sup> 32.08 <sup>s</sup>	+01 <sup>°</sup> 54 <sup>m</sup> 24.12 <sup>s</sup>	2.3666	14	1	20.68	20.40	20.15	19.76	point-like	FORS
100126868	10 <sup>h</sup> 03 <sup>m</sup> 08.80 <sup>s</sup>	+01 <sup>°</sup> 23 <sup>m</sup> 16.56 <sup>s</sup>	2.3302	14	1	...	...	...	20.34	point-like	...
100578140	10 <sup>h</sup> 04 <sup>m</sup> 29.89 <sup>s</sup>	+02 <sup>°</sup> 28 <sup>m</sup> 21.44 <sup>s</sup>	2.2884	13	2	22.13	22.08	22.50	21.71	point-like	...
100566130	10 <sup>h</sup> 04 <sup>m</sup> 15.12 <sup>s</sup>	+02 <sup>°</sup> 25 <sup>m</sup> 42.17 <sup>s</sup>	2.2030	14	2	22.73	22.37	22.48	21.69	point-like	...
100123590	10 <sup>h</sup> 04 <sup>m</sup> 46.72 <sup>s</sup>	+01 <sup>°</sup> 22 <sup>m</sup> 39.10 <sup>s</sup>	2.0963	13	1	...	...	...	21.47	point-like	...
100530812	10 <sup>h</sup> 04 <sup>m</sup> 48.64 <sup>s</sup>	+02 <sup>°</sup> 19 <sup>m</sup> 44.38 <sup>s</sup>	2.0201	14	2	21.00	20.53	20.75	20.39	point-like	...
100447217	10 <sup>h</sup> 03 <sup>m</sup> 12.70 <sup>s</sup>	+02 <sup>°</sup> 08 <sup>m</sup> 50.66 <sup>s</sup>	1.8900	13	2	22.71	22.50	22.51	21.91	point-like	...
100113463	10 <sup>h</sup> 04 <sup>m</sup> 07.25 <sup>s</sup>	+01 <sup>°</sup> 20 <sup>m</sup> 38.90 <sup>s</sup>	1.8436	14	1	...	...	...	20.47	point-like	2QZ
100110223	10 <sup>h</sup> 02 <sup>m</sup> 48.14 <sup>s</sup>	+01 <sup>°</sup> 20 <sup>m</sup> 02.29 <sup>s</sup>	1.8255	13	1	...	...	...	21.29	point-like	...
100122852	10 <sup>h</sup> 02 <sup>m</sup> 11.17 <sup>s</sup>	+01 <sup>°</sup> 22 <sup>m</sup> 28.58 <sup>s</sup>	1.8007	14	1	...	...	...	19.86	point-like	2QZ
100507363	10 <sup>h</sup> 04 <sup>m</sup> 50.02 <sup>s</sup>	+02 <sup>°</sup> 16 <sup>m</sup> 42.21 <sup>s</sup>	1.7842	14	2	22.71	22.47	22.18	21.64	extended	...
100451895	10 <sup>h</sup> 04 <sup>m</sup> 38.01 <sup>s</sup>	+02 <sup>°</sup> 09 <sup>m</sup> 25.07 <sup>s</sup>	1.7806	13	1	20.46	20.31	20.36	20.03	point-like	...
100232259	10 <sup>h</sup> 03 <sup>m</sup> 30.37 <sup>s</sup>	+01 <sup>°</sup> 38 <sup>m</sup> 51.18 <sup>s</sup>	1.7647	14	1	21.37	21.30	21.33	21.09	point-like	FORS
100290682	10 <sup>h</sup> 03 <sup>m</sup> 11.33 <sup>s</sup>	+01 <sup>°</sup> 47 <sup>m</sup> 01.56 <sup>s</sup>	1.5487	14	1	...	...	...	21.45	extended	FORS
100046262	10 <sup>h</sup> 07 <sup>m</sup> 34.87 <sup>s</sup>	+01 <sup>°</sup> 07 <sup>m</sup> 13.95 <sup>s</sup>	1.4627	14	2	...	...	...	20.89	point-like	SDSS
100198426	10 <sup>h</sup> 03 <sup>m</sup> 42.73 <sup>s</sup>	+01 <sup>°</sup> 34 <sup>m</sup> 12.51 <sup>s</sup>	1.3372	14	1	23.32	22.96	22.82	22.09	point-like	...
100139500	10 <sup>h</sup> 02 <sup>m</sup> 57.37 <sup>s</sup>	+01 <sup>°</sup> 25 <sup>m</sup> 40.38 <sup>s</sup>	1.2478	13	1	...	...	...	20.96	point-like	...
100327652	10 <sup>h</sup> 03 <sup>m</sup> 13.81 <sup>s</sup>	+01 <sup>°</sup> 52 <sup>m</sup> 13.97 <sup>s</sup>	1.2173	14	1	23.85	23.43	22.90	22.39	extended	FORS
100048462	10 <sup>h</sup> 03 <sup>m</sup> 13.77 <sup>s</sup>	+01 <sup>°</sup> 07 <sup>m</sup> 41.06 <sup>s</sup>	1.2028	13	2	...	...	...	20.43	point-like	...
100184041	10 <sup>h</sup> 03 <sup>m</sup> 49.53 <sup>s</sup>	+01 <sup>°</sup> 32 <sup>m</sup> 12.26 <sup>s</sup>	1.2028	14	1	23.44	22.94	22.88	21.87	point-like	...
100210521	10 <sup>h</sup> 03 <sup>m</sup> 27.33 <sup>s</sup>	+01 <sup>°</sup> 35 <sup>m</sup> 50.91 <sup>s</sup>	1.1723	14	1	22.05	21.73	21.56	21.58	point-like	...
100338914	10 <sup>h</sup> 04 <sup>m</sup> 13.45 <sup>s</sup>	+01 <sup>°</sup> 53 <sup>m</sup> 41.38 <sup>s</sup>	1.1584	14	1	20.15	19.80	19.78	19.73	extended	...
100241696	10 <sup>h</sup> 04 <sup>m</sup> 11.84 <sup>s</sup>	+01 <sup>°</sup> 40 <sup>m</sup> 06.47 <sup>s</sup>	1.1112	13	1	22.59	21.89	22.19	21.95	point-like	...
100190464	10 <sup>h</sup> 04 <sup>m</sup> 25.14 <sup>s</sup>	+01 <sup>°</sup> 33 <sup>m</sup> 07.74 <sup>s</sup>	1.0760	14	1	22.98	22.38	22.41	21.66	extended	...
100641029	10 <sup>h</sup> 04 <sup>m</sup> 00.44 <sup>s</sup>	+02 <sup>°</sup> 41 <sup>m</sup> 22.83 <sup>s</sup>	0.8322	14	2	22.18	21.52	21.70	21.08	extended	...
1400+05	Wide mode	28 AGN									
140431249	13 <sup>h</sup> 55 <sup>m</sup> 47.47 <sup>s</sup>	+05 <sup>°</sup> 11 <sup>m</sup> 21.63 <sup>s</sup>	3.8452	14	2	...	...	...	21.42	...	...
140465826	13 <sup>h</sup> 58 <sup>m</sup> 37.30 <sup>s</sup>	+05 <sup>°</sup> 17 <sup>m</sup> 14.44 <sup>s</sup>	3.2900	14	2	20.92	19.92	19.89	20.11	...	...
140191403	13 <sup>h</sup> 57 <sup>m</sup> 44.60 <sup>s</sup>	+04 <sup>°</sup> 34 <sup>m</sup> 42.28 <sup>s</sup>	3.1704	14	2	...	...	21.60	22.10	...	...
140156421	13 <sup>h</sup> 57 <sup>m</sup> 54.50 <sup>s</sup>	+04 <sup>°</sup> 29 <sup>m</sup> 28.69 <sup>s</sup>	3.1464	14	2	22.76	21.78	21.80	21.74	...	...
140493205	13 <sup>h</sup> 57 <sup>m</sup> 36.79 <sup>s</sup>	+05 <sup>°</sup> 21 <sup>m</sup> 53.11 <sup>s</sup>	2.8650	14	2	...	21.82	21.69	21.61	...	...
140040016	13 <sup>h</sup> 58 <sup>m</sup> 30.18 <sup>s</sup>	+04 <sup>°</sup> 10 <sup>m</sup> 08.54 <sup>s</sup>	2.8379	13	2	21.29	21.44	21.45	21.49	...	...
140432542	13 <sup>h</sup> 55 <sup>m</sup> 41.68 <sup>s</sup>	+05 <sup>°</sup> 11 <sup>m</sup> 36.10 <sup>s</sup>	2.8000	14	2	...	...	...	21.80	...	...
140523286	13 <sup>h</sup> 58 <sup>m</sup> 30.57 <sup>s</sup>	+05 <sup>°</sup> 27 <sup>m</sup> 02.35 <sup>s</sup>	2.7100	13	2	20.50	20.24	19.95	19.92	...	...
140373668	13 <sup>h</sup> 55 <sup>m</sup> 52.45 <sup>s</sup>	+05 <sup>°</sup> 01 <sup>m</sup> 24.81 <sup>s</sup>	2.3130	14	2	...	...	...	20.98	...	...
140338871	13 <sup>h</sup> 55 <sup>m</sup> 40.98 <sup>s</sup>	+04 <sup>°</sup> 56 <sup>m</sup> 17.57 <sup>s</sup>	2.1084	14	2	...	...	...	22.23	...	...
140166360	13 <sup>h</sup> 55 <sup>m</sup> 55.44 <sup>s</sup>	+04 <sup>°</sup> 31 <sup>m</sup> 07.70 <sup>s</sup>	2.1000	14	2	...	...	...	21.30	...	...
140166951	13 <sup>h</sup> 55 <sup>m</sup> 54.92 <sup>s</sup>	+04 <sup>°</sup> 31 <sup>m</sup> 14.32 <sup>s</sup>	1.9912	14	2	...	...	...	21.79	...	...

**Table B.1.** continued.

Object ID (1)	$\alpha_{J2000}$ (2)	$\delta_{J2000}$ (3)	$z$ (4)	Flag (5)	Epoch (6)	$B_{AB}$ (7)	$V_{AB}$ (8)	$R_{AB}$ (9)	$I_{AB}$ (10)	Morphology (11)	Remark (12)
140265284	13 <sup>h</sup> 55 <sup>m</sup> 42.76 <sup>s</sup>	+04 <sup>o</sup> 45 <sup>m</sup> 46.62 <sup>s</sup>	1.8549	13	2	...	...	...	21.41	...	...
140520998	13 <sup>h</sup> 57 <sup>m</sup> 53.93 <sup>s</sup>	+05 <sup>o</sup> 26 <sup>m</sup> 39.07 <sup>s</sup>	1.8293	13	2	...	21.09	21.10	20.84	...	...
140363408	13 <sup>h</sup> 58 <sup>m</sup> 36.16 <sup>s</sup>	+04 <sup>o</sup> 59 <sup>m</sup> 49.74 <sup>s</sup>	1.8260	13	2	22.12	21.86	21.72	21.81	...	...
140495178	13 <sup>h</sup> 59 <sup>m</sup> 33.29 <sup>s</sup>	+05 <sup>o</sup> 22 <sup>m</sup> 09.08 <sup>s</sup>	1.8241	13	2	21.77	21.05	20.71	20.75	...	...
140433507	14 <sup>h</sup> 00 <sup>m</sup> 33.04 <sup>s</sup>	+05 <sup>o</sup> 11 <sup>m</sup> 48.09 <sup>s</sup>	1.7645	13	2	21.20	21.14	21.56	21.09	...	...
140338689	14 <sup>h</sup> 01 <sup>m</sup> 34.46 <sup>s</sup>	+04 <sup>o</sup> 56 <sup>m</sup> 17.27 <sup>s</sup>	1.4420	14	2	22.01	21.44	21.03	20.69	...	...
140441955	13 <sup>h</sup> 58 <sup>m</sup> 28.26 <sup>s</sup>	+05 <sup>o</sup> 13 <sup>m</sup> 11.92 <sup>s</sup>	1.4290	13	2	23.15	21.94	21.47	22.01	...	...
140305471	13 <sup>h</sup> 58 <sup>m</sup> 16.55 <sup>s</sup>	+04 <sup>o</sup> 51 <sup>m</sup> 35.36 <sup>s</sup>	1.3703	13	2	21.04	21.05	21.47	21.02	...	...
140222324	13 <sup>h</sup> 57 <sup>m</sup> 56.92 <sup>s</sup>	+04 <sup>o</sup> 39 <sup>m</sup> 20.01 <sup>s</sup>	1.3053	14	2	...	22.01	21.88	21.66	...	...
140433055	13 <sup>h</sup> 56 <sup>m</sup> 49.40 <sup>s</sup>	+05 <sup>o</sup> 11 <sup>m</sup> 43.77 <sup>s</sup>	1.2077	13	2	...	...	21.91	22.28	...	...
140306523	13 <sup>h</sup> 56 <sup>m</sup> 49.91 <sup>s</sup>	+04 <sup>o</sup> 51 <sup>m</sup> 37.87 <sup>s</sup>	1.1902	13	2	...	...	19.72	20.06	...	...
140192158	13 <sup>h</sup> 58 <sup>m</sup> 35.43 <sup>s</sup>	+04 <sup>o</sup> 34 <sup>m</sup> 49.21 <sup>s</sup>	1.1265	13	2	22.79	22.34	21.97	22.06	...	...
140443623	13 <sup>h</sup> 58 <sup>m</sup> 13.27 <sup>s</sup>	+05 <sup>o</sup> 13 <sup>m</sup> 28.45 <sup>s</sup>	1.1195	14	2	22.44	21.98	22.05	21.43	...	...
140278593	13 <sup>h</sup> 59 <sup>m</sup> 44.60 <sup>s</sup>	+04 <sup>o</sup> 47 <sup>m</sup> 40.37 <sup>s</sup>	1.0460	13	2	20.68	20.18	20.68	20.45	...	...
140215102	13 <sup>h</sup> 56 <sup>m</sup> 39.41 <sup>s</sup>	+04 <sup>o</sup> 38 <sup>m</sup> 14.32 <sup>s</sup>	0.5487	14	2	...	...	21.14	20.94	...	...
140360727	13 <sup>h</sup> 55 <sup>m</sup> 44.37 <sup>s</sup>	+04 <sup>o</sup> 59 <sup>m</sup> 15.10 <sup>s</sup>	0.1236	14	2	...	...	...	18.58	...	...
2217+00	Wide mode	105 AGN									
220567224	22 <sup>h</sup> 16 <sup>m</sup> 44.02 <sup>s</sup>	+00 <sup>o</sup> 13 <sup>m</sup> 48.54 <sup>s</sup>	5.0042	14	1	...	22.90	21.66	20.07	point-like	...
220437943	22 <sup>h</sup> 20 <sup>m</sup> 50.80 <sup>s</sup>	+00 <sup>o</sup> 19 <sup>m</sup> 59.53 <sup>s</sup>	4.6694	14	2	...	21.83	20.60	20.10	point-like	...
220490264	22 <sup>h</sup> 17 <sup>m</sup> 05.70 <sup>s</sup>	-00 <sup>o</sup> 13 <sup>m</sup> 07.28 <sup>s</sup>	4.6677	14	2	...	21.94	...	20.42	point-like	...
220183694	22 <sup>h</sup> 20 <sup>m</sup> 32.47 <sup>s</sup>	+00 <sup>o</sup> 25 <sup>m</sup> 38.16 <sup>s</sup>	4.1928	14	2	23.69	21.33	20.11	20.14	point-like	...
220267678	22 <sup>h</sup> 21 <sup>m</sup> 32.55 <sup>s</sup>	+01 <sup>o</sup> 00 <sup>m</sup> 05.84 <sup>s</sup>	3.8331	14	2	...	...	...	21.34	point-like	...
220270600	22 <sup>h</sup> 21 <sup>m</sup> 50.78 <sup>s</sup>	+01 <sup>o</sup> 01 <sup>m</sup> 02.34 <sup>s</sup>	3.7351	14	2	...	...	...	22.34	extended	...
220010371	22 <sup>h</sup> 14 <sup>m</sup> 28.40 <sup>s</sup>	+00 <sup>o</sup> 27 <sup>m</sup> 32.40 <sup>s</sup>	3.6952	214	1	...	...	...	21.78	point-like	...
220055529	22 <sup>h</sup> 15 <sup>m</sup> 54.10 <sup>s</sup>	+00 <sup>o</sup> 40 <sup>m</sup> 55.47 <sup>s</sup>	3.5941	13	1	...	...	...	21.42	point-like	...
220300661	22 <sup>h</sup> 19 <sup>m</sup> 32.96 <sup>s</sup>	+01 <sup>o</sup> 10 <sup>m</sup> 46.87 <sup>s</sup>	3.5879	214	2	...	...	...	19.59	extended	...
220576935	22 <sup>h</sup> 17 <sup>m</sup> 22.27 <sup>s</sup>	+00 <sup>o</sup> 16 <sup>m</sup> 40.41 <sup>s</sup>	3.3650	14	2	22.10	20.86	20.92	20.79	point-like	...
220359141	22 <sup>h</sup> 19 <sup>m</sup> 54.56 <sup>s</sup>	-00 <sup>o</sup> 15 <sup>m</sup> 46.22 <sup>s</sup>	3.1582	214	2	...	...	...	22.64	extended	...
220157547	22 <sup>h</sup> 13 <sup>m</sup> 51.40 <sup>s</sup>	+01 <sup>o</sup> 11 <sup>m</sup> 11.53 <sup>s</sup>	3.1518	14	2	...	...	...	22.19	extended	...
220133794	22 <sup>h</sup> 18 <sup>m</sup> 00.48 <sup>s</sup>	+01 <sup>o</sup> 04 <sup>m</sup> 07.32 <sup>s</sup>	3.1473	14	2	...	...	...	22.16	point-like	...
220617869	22 <sup>h</sup> 18 <sup>m</sup> 52.17 <sup>s</sup>	+00 <sup>o</sup> 34 <sup>m</sup> 50.72 <sup>s</sup>	3.1334	14	2	24.11	23.16	22.27	22.25	point-like	...
220215380	22 <sup>h</sup> 19 <sup>m</sup> 43.32 <sup>s</sup>	+00 <sup>o</sup> 41 <sup>m</sup> 19.18 <sup>s</sup>	3.1300	14	2	19.91	19.09	18.98	19.01	point-like	...
220576817	22 <sup>h</sup> 15 <sup>m</sup> 09.17 <sup>s</sup>	+00 <sup>o</sup> 16 <sup>m</sup> 42.38 <sup>s</sup>	3.0957	14	1	...	...	...	21.81	point-like	...
220309346	22 <sup>h</sup> 20 <sup>m</sup> 43.12 <sup>s</sup>	+01 <sup>o</sup> 13 <sup>m</sup> 51.19 <sup>s</sup>	3.0899	14	2	...	...	...	22.11	point-like	...
220391155	22 <sup>h</sup> 18 <sup>m</sup> 54.28 <sup>s</sup>	-00 <sup>o</sup> 00 <sup>m</sup> 58.53 <sup>s</sup>	3.0870	14	2	21.78	21.03	20.98	20.89	point-like	...
220205172	22 <sup>h</sup> 19 <sup>m</sup> 58.22 <sup>s</sup>	+00 <sup>o</sup> 37 <sup>m</sup> 10.08 <sup>s</sup>	3.0759	14	2	19.94	19.30	19.06	19.06	point-like	...
220575888	22 <sup>h</sup> 17 <sup>m</sup> 36.55 <sup>s</sup>	+00 <sup>o</sup> 16 <sup>m</sup> 23.09 <sup>s</sup>	3.0755	14	1	22.16	21.50	21.23	21.25	point-like	...
220133609	22 <sup>h</sup> 16 <sup>m</sup> 36.81 <sup>s</sup>	+01 <sup>o</sup> 04 <sup>m</sup> 02.27 <sup>s</sup>	3.0507	14	2	...	...	...	20.31	extended	...
220580912	22 <sup>h</sup> 15 <sup>m</sup> 56.66 <sup>s</sup>	+00 <sup>o</sup> 17 <sup>m</sup> 52.28 <sup>s</sup>	3.0432	13	1	...	...	...	22.10	point-like	...
220410190	22 <sup>h</sup> 18 <sup>m</sup> 58.92 <sup>s</sup>	+00 <sup>o</sup> 07 <sup>m</sup> 12.45 <sup>s</sup>	3.0335	14	2	23.15	22.48	22.03	21.70	point-like	...
220056847	22 <sup>h</sup> 14 <sup>m</sup> 48.77 <sup>s</sup>	+00 <sup>o</sup> 41 <sup>m</sup> 16.67 <sup>s</sup>	3.0015	14	1	...	...	...	21.38	point-like	...
220044408	22 <sup>h</sup> 17 <sup>m</sup> 34.47 <sup>s</sup>	+00 <sup>o</sup> 37 <sup>m</sup> 33.52 <sup>s</sup>	2.9096	214	1	21.65	21.54	21.46	21.18	point-like	FORS
220181962	22 <sup>h</sup> 19 <sup>m</sup> 36.35 <sup>s</sup>	+00 <sup>o</sup> 24 <sup>m</sup> 34.58 <sup>s</sup>	2.8558	14	2	18.86	18.76	18.60	18.59	extended	...
220208314	22 <sup>h</sup> 20 <sup>m</sup> 59.50 <sup>s</sup>	+00 <sup>o</sup> 38 <sup>m</sup> 40.82 <sup>s</sup>	2.8204	14	2	23.33	22.64	21.74	21.57	point-like	...
220514118	22 <sup>h</sup> 17 <sup>m</sup> 34.45 <sup>s</sup>	-00 <sup>o</sup> 03 <sup>m</sup> 10.88 <sup>s</sup>	2.8136	14	2	23.65	23.05	...	22.19	point-like	...
220556037	22 <sup>h</sup> 17 <sup>m</sup> 05.53 <sup>s</sup>	+00 <sup>o</sup> 10 <sup>m</sup> 19.85 <sup>s</sup>	2.7422	14	1	20.52	20.29	19.63	19.45	point-like	...
220372036	22 <sup>h</sup> 20 <sup>m</sup> 02.78 <sup>s</sup>	-00 <sup>o</sup> 10 <sup>m</sup> 09.28 <sup>s</sup>	2.7081	14	2	...	...	...	21.41	point-like	...
220141562	22 <sup>h</sup> 17 <sup>m</sup> 34.71 <sup>s</sup>	+01 <sup>o</sup> 06 <sup>m</sup> 26.48 <sup>s</sup>	2.6899	13	2	...	...	...	22.12	point-like	...
220001963	22 <sup>h</sup> 13 <sup>m</sup> 51.58 <sup>s</sup>	+00 <sup>o</sup> 25 <sup>m</sup> 01.30 <sup>s</sup>	2.6801	14	1	...	...	...	22.19	point-like	...
220457748	22 <sup>h</sup> 14 <sup>m</sup> 09.13 <sup>s</sup>	-00 <sup>o</sup> 27 <sup>m</sup> 17.14 <sup>s</sup>	2.6490	13	2	...	...	...	20.70	point-like	...
220098629	22 <sup>h</sup> 18 <sup>m</sup> 01.51 <sup>s</sup>	+00 <sup>o</sup> 53 <sup>m</sup> 19.83 <sup>s</sup>	2.5790	14	1	...	...	...	21.71	point-like	FORS
220404101	22 <sup>h</sup> 21 <sup>m</sup> 29.86 <sup>s</sup>	+00 <sup>o</sup> 04 <sup>m</sup> 30.35 <sup>s</sup>	2.4827	14	2	19.27	19.09	19.08	19.19	point-like	...
220446330	22 <sup>h</sup> 20 <sup>m</sup> 07.75 <sup>s</sup>	+00 <sup>o</sup> 23 <sup>m</sup> 32.53 <sup>s</sup>	2.4149	13	2	21.67	21.03	20.68	20.39	point-like	...
220544855	22 <sup>h</sup> 17 <sup>m</sup> 39.71 <sup>s</sup>	+00 <sup>o</sup> 06 <sup>m</sup> 52.80 <sup>s</sup>	2.2934	14	1	21.97	21.61	21.00	20.91	extended	FORS
220401794	22 <sup>h</sup> 20 <sup>m</sup> 57.43 <sup>s</sup>	+00 <sup>o</sup> 03 <sup>m</sup> 30.33 <sup>s</sup>	2.2543	14	2	19.17	18.92	18.69	18.65	point-like	...
220235977	22 <sup>h</sup> 20 <sup>m</sup> 52.76 <sup>s</sup>	+00 <sup>o</sup> 49 <sup>m</sup> 18.10 <sup>s</sup>	2.1919	14	2	21.06	20.92	20.97	20.74	point-like	...
220567863	22 <sup>h</sup> 16 <sup>m</sup> 27.06 <sup>s</sup>	+00 <sup>o</sup> 14 <sup>m</sup> 02.32 <sup>s</sup>	2.1610	14	1	...	...	21.10	20.79	point-like	...
220130245	22 <sup>h</sup> 17 <sup>m</sup> 52.14 <sup>s</sup>	+01 <sup>o</sup> 02 <sup>m</sup> 59.22 <sup>s</sup>	2.1502	14	2	...	...	...	19.65	point-like	...
220459956	22 <sup>h</sup> 17 <sup>m</sup> 11.07 <sup>s</sup>	-00 <sup>o</sup> 26 <sup>m</sup> 19.47 <sup>s</sup>	2.1220	14	2	...	...	...	21.03	point-like	...
220470488	22 <sup>h</sup> 13 <sup>m</sup> 55.40 <sup>s</sup>	-00 <sup>o</sup> 21 <sup>m</sup> 40.75 <sup>s</sup>	2.0405	14	2	...	...	...	21.20	point-like	...

**Table B.1.** continued.

Object ID (1)	$\alpha_{J2000}$ (2)	$\delta_{J2000}$ (3)	$z$ (4)	Flag (5)	Epoch (6)	$B_{AB}$ (7)	$V_{AB}$ (8)	$R_{AB}$ (9)	$I_{AB}$ (10)	Morphology (11)	Remark (12)
220463685	22 <sup>h</sup> 17 <sup>m</sup> 59.99 <sup>s</sup>	-00 <sup>o</sup> 24 <sup>m</sup> 40.20 <sup>s</sup>	2.0300	14	2	...	...	...	21.03	point-like	...
220125352	22 <sup>h</sup> 14 <sup>m</sup> 30.06 <sup>s</sup>	+01 <sup>o</sup> 01 <sup>m</sup> 33.05 <sup>s</sup>	2.0128	14	2	...	...	...	21.19	point-like	...
220531803	22 <sup>h</sup> 13 <sup>m</sup> 55.52 <sup>s</sup>	+00 <sup>o</sup> 02 <sup>m</sup> 44.37 <sup>s</sup>	1.9932	14	2	...	...	...	21.75	point-like	...
220562230	22 <sup>h</sup> 17 <sup>m</sup> 47.95 <sup>s</sup>	+00 <sup>o</sup> 12 <sup>m</sup> 23.74 <sup>s</sup>	1.9711	13	2	21.95	21.81	21.94	21.32	point-like	...
220365504	22 <sup>h</sup> 20 <sup>m</sup> 52.40 <sup>s</sup>	-00 <sup>o</sup> 13 <sup>m</sup> 02.95 <sup>s</sup>	1.9447	13	2	...	...	...	21.69	point-like	...
220551387	22 <sup>h</sup> 16 <sup>m</sup> 35.64 <sup>s</sup>	+00 <sup>o</sup> 09 <sup>m</sup> 04.83 <sup>s</sup>	1.8810	13	2	21.23	21.69	21.04	21.42	point-like	...
220082140	22 <sup>h</sup> 15 <sup>m</sup> 32.40 <sup>s</sup>	+00 <sup>o</sup> 48 <sup>m</sup> 36.29 <sup>s</sup>	1.8484	14	1	...	...	...	20.59	point-like	FORS
220090821	22 <sup>h</sup> 15 <sup>m</sup> 46.25 <sup>s</sup>	+00 <sup>o</sup> 50 <sup>m</sup> 58.51 <sup>s</sup>	1.8326	13	1	...	...	...	20.40	point-like	...
220308643	22 <sup>h</sup> 20 <sup>m</sup> 02.34 <sup>s</sup>	+01 <sup>o</sup> 13 <sup>m</sup> 37.14 <sup>s</sup>	1.8007	13	2	...	...	...	21.75	point-like	...
220438495	22 <sup>h</sup> 20 <sup>m</sup> 04.64 <sup>s</sup>	+00 <sup>o</sup> 20 <sup>m</sup> 17.30 <sup>s</sup>	1.7738	13	2	23.02	22.54	22.25	21.82	point-like	...
220370320	22 <sup>h</sup> 18 <sup>m</sup> 13.11 <sup>s</sup>	-00 <sup>o</sup> 11 <sup>m</sup> 00.04 <sup>s</sup>	1.7445	13	2	...	20.50	...	20.06	point-like	...
220409734	22 <sup>h</sup> 18 <sup>m</sup> 16.60 <sup>s</sup>	+00 <sup>o</sup> 07 <sup>m</sup> 01.37 <sup>s</sup>	1.7415	13	2	23.23	22.90	22.41	21.74	point-like	...
220159199	22 <sup>h</sup> 15 <sup>m</sup> 57.05 <sup>s</sup>	+01 <sup>o</sup> 11 <sup>m</sup> 40.39 <sup>s</sup>	1.7217	13	2	...	...	...	22.04	point-like	...
220427244	22 <sup>h</sup> 21 <sup>m</sup> 28.67 <sup>s</sup>	+00 <sup>o</sup> 14 <sup>m</sup> 44.01 <sup>s</sup>	1.6815	13	2	20.83	20.57	20.33	20.28	point-like	...
220371301	22 <sup>h</sup> 20 <sup>m</sup> 28.72 <sup>s</sup>	-00 <sup>o</sup> 10 <sup>m</sup> 28.43 <sup>s</sup>	1.6452	13	2	...	...	...	22.06	point-like	...
220566905	22 <sup>h</sup> 14 <sup>m</sup> 02.39 <sup>s</sup>	+00 <sup>o</sup> 13 <sup>m</sup> 49.58 <sup>s</sup>	1.5285	13	1	...	...	...	22.27	point-like	...
220610034	22 <sup>h</sup> 18 <sup>m</sup> 14.20 <sup>s</sup>	+00 <sup>o</sup> 20 <sup>m</sup> 49.73 <sup>s</sup>	1.5135	14	1	20.77	20.86	20.60	20.54	extended	FORS
220327763	22 <sup>h</sup> 18 <sup>m</sup> 29.94 <sup>s</sup>	-00 <sup>o</sup> 30 <sup>m</sup> 35.89 <sup>s</sup>	1.5007	13	2	...	...	...	21.21	point-like	...
220568559	22 <sup>h</sup> 14 <sup>m</sup> 43.23 <sup>s</sup>	+00 <sup>o</sup> 14 <sup>m</sup> 16.29 <sup>s</sup>	1.4980	13	1	...	...	...	22.10	point-like	...
220609820	22 <sup>h</sup> 18 <sup>m</sup> 29.04 <sup>s</sup>	+00 <sup>o</sup> 20 <sup>m</sup> 24.32 <sup>s</sup>	1.4794	14	1	22.04	21.86	21.52	21.52	extended	FORS
220419246	22 <sup>h</sup> 20 <sup>m</sup> 12.52 <sup>s</sup>	+00 <sup>o</sup> 10 <sup>m</sup> 51.96 <sup>s</sup>	1.4786	13	2	21.54	21.54	20.80	20.62	point-like	...
220041929	22 <sup>h</sup> 15 <sup>m</sup> 09.54 <sup>s</sup>	+00 <sup>o</sup> 36 <sup>m</sup> 39.11 <sup>s</sup>	1.4751	13	1	...	...	...	18.23	extended	...
220376198	22 <sup>h</sup> 21 <sup>m</sup> 30.08 <sup>s</sup>	-00 <sup>o</sup> 08 <sup>m</sup> 18.91 <sup>s</sup>	1.4687	13	2	...	...	...	21.63	point-like	...
220377744	22 <sup>h</sup> 21 <sup>m</sup> 44.12 <sup>s</sup>	-00 <sup>o</sup> 07 <sup>m</sup> 39.17 <sup>s</sup>	1.4653	14	2	...	...	...	21.06	point-like	...
220469918	22 <sup>h</sup> 15 <sup>m</sup> 31.85 <sup>s</sup>	-00 <sup>o</sup> 21 <sup>m</sup> 54.28 <sup>s</sup>	1.4600	14	2	...	...	...	21.74	extended	...
220326578	22 <sup>h</sup> 20 <sup>m</sup> 34.72 <sup>s</sup>	-00 <sup>o</sup> 31 <sup>m</sup> 10.93 <sup>s</sup>	1.3913	14	2	...	...	...	22.07	extended	...
220554600	22 <sup>h</sup> 17 <sup>m</sup> 36.64 <sup>s</sup>	+00 <sup>o</sup> 10 <sup>m</sup> 05.86 <sup>s</sup>	1.3689	14	1	21.21	21.00	20.62	20.65	point-like	FORS
220093875	22 <sup>h</sup> 17 <sup>m</sup> 48.64 <sup>s</sup>	+00 <sup>o</sup> 51 <sup>m</sup> 50.39 <sup>s</sup>	1.3365	14	1	...	...	...	21.83	point-like	FORS
220542377	22 <sup>h</sup> 17 <sup>m</sup> 10.42 <sup>s</sup>	+00 <sup>o</sup> 06 <sup>m</sup> 04.72 <sup>s</sup>	1.3097	13	1	22.24	21.95	21.53	21.12	point-like	...
220054185	22 <sup>h</sup> 15 <sup>m</sup> 47.71 <sup>s</sup>	+00 <sup>o</sup> 40 <sup>m</sup> 29.96 <sup>s</sup>	1.3057	14	1	...	...	...	21.59	point-like	...
220591287	22 <sup>h</sup> 16 <sup>m</sup> 49.05 <sup>s</sup>	+00 <sup>o</sup> 20 <sup>m</sup> 46.27 <sup>s</sup>	1.2968	14	1	23.47	23.32	22.67	22.30	extended	FORS
220525793	22 <sup>h</sup> 14 <sup>m</sup> 05.51 <sup>s</sup>	+00 <sup>o</sup> 00 <sup>m</sup> 39.28 <sup>s</sup>	1.2940	13	2	...	...	...	19.01	point-like	...
220154139	22 <sup>h</sup> 14 <sup>m</sup> 33.65 <sup>s</sup>	+01 <sup>o</sup> 10 <sup>m</sup> 09.87 <sup>s</sup>	1.2903	13	2	...	...	...	22.23	extended	...
220247296	22 <sup>h</sup> 21 <sup>m</sup> 00.32 <sup>s</sup>	+00 <sup>o</sup> 53 <sup>m</sup> 20.89 <sup>s</sup>	1.2846	13	2	...	...	...	21.41	point-like	...
220613346	22 <sup>h</sup> 18 <sup>m</sup> 33.73 <sup>s</sup>	+00 <sup>o</sup> 27 <sup>m</sup> 09.76 <sup>s</sup>	1.2530	14	1	21.63	21.25	20.41	20.39	extended	FORS
220081925	22 <sup>h</sup> 18 <sup>m</sup> 00.42 <sup>s</sup>	+00 <sup>o</sup> 48 <sup>m</sup> 31.41 <sup>s</sup>	1.2167	13	1	22.79	22.40	21.80	21.68	extended	...
220375302	22 <sup>h</sup> 21 <sup>m</sup> 32.17 <sup>s</sup>	-00 <sup>o</sup> 08 <sup>m</sup> 43.44 <sup>s</sup>	1.2082	13	2	...	...	...	21.70	extended	...
220255701	22 <sup>h</sup> 19 <sup>m</sup> 10.54 <sup>s</sup>	+00 <sup>o</sup> 56 <sup>m</sup> 06.93 <sup>s</sup>	1.1932	14	2	...	...	...	19.64	point-like	...
220567825	22 <sup>h</sup> 15 <sup>m</sup> 08.48 <sup>s</sup>	+00 <sup>o</sup> 14 <sup>m</sup> 04.38 <sup>s</sup>	1.1601	13	1	...	...	...	21.07	point-like	...
220561414	22 <sup>h</sup> 17 <sup>m</sup> 38.41 <sup>s</sup>	+00 <sup>o</sup> 12 <sup>m</sup> 07.01 <sup>s</sup>	1.1243	14	2	20.60	20.24	20.09	19.98	point-like	...
220357650	22 <sup>h</sup> 19 <sup>m</sup> 58.50 <sup>s</sup>	-00 <sup>o</sup> 16 <sup>m</sup> 23.97 <sup>s</sup>	1.1228	13	2	...	...	...	22.21	point-like	...
220458211	22 <sup>h</sup> 17 <sup>m</sup> 58.70 <sup>s</sup>	-00 <sup>o</sup> 27 <sup>m</sup> 07.43 <sup>s</sup>	1.1049	13	2	...	...	...	20.54	point-like	...
220107230	22 <sup>h</sup> 16 <sup>m</sup> 56.10 <sup>s</sup>	+00 <sup>o</sup> 56 <sup>m</sup> 00.77 <sup>s</sup>	1.0937	13	1	...	...	...	21.63	point-like	...
220463317	22 <sup>h</sup> 13 <sup>m</sup> 56.02 <sup>s</sup>	-00 <sup>o</sup> 24 <sup>m</sup> 55.47 <sup>s</sup>	1.0655	13	2	...	...	...	19.45	point-like	...
220152300	22 <sup>h</sup> 15 <sup>m</sup> 04.35 <sup>s</sup>	+01 <sup>o</sup> 09 <sup>m</sup> 35.55 <sup>s</sup>	1.0380	13	2	...	...	...	20.61	point-like	...
220586430	22 <sup>h</sup> 14 <sup>m</sup> 34.82 <sup>s</sup>	+00 <sup>o</sup> 19 <sup>m</sup> 24.18 <sup>s</sup>	1.0285	14	1	...	...	...	20.35	point-like	...
220125074	22 <sup>h</sup> 17 <sup>m</sup> 56.93 <sup>s</sup>	+01 <sup>o</sup> 01 <sup>m</sup> 19.87 <sup>s</sup>	0.8640	14	2	...	...	...	18.04	extended	...
220149257	22 <sup>h</sup> 17 <sup>m</sup> 24.33 <sup>s</sup>	+01 <sup>o</sup> 08 <sup>m</sup> 41.68 <sup>s</sup>	0.8477	14	2	...	...	...	21.10	point-like	...
220294100	22 <sup>h</sup> 18 <sup>m</sup> 15.60 <sup>s</sup>	+01 <sup>o</sup> 08 <sup>m</sup> 42.69 <sup>s</sup>	0.7411	14	2	...	...	...	18.13	point-like	...
220504239	22 <sup>h</sup> 16 <sup>m</sup> 23.77 <sup>s</sup>	-00 <sup>o</sup> 07 <sup>m</sup> 28.36 <sup>s</sup>	0.7290	14	2	...	...	...	20.07	point-like	...
220215958	22 <sup>h</sup> 19 <sup>m</sup> 51.28 <sup>s</sup>	+00 <sup>o</sup> 41 <sup>m</sup> 35.99 <sup>s</sup>	0.6559	14	2	22.07	21.87	21.38	21.20	point-like	...
220212912	22 <sup>h</sup> 19 <sup>m</sup> 07.95 <sup>s</sup>	+00 <sup>o</sup> 40 <sup>m</sup> 23.90 <sup>s</sup>	0.6146	14	2	20.43	20.15	19.80	19.60	extended	...
220464758	22 <sup>h</sup> 17 <sup>m</sup> 50.50 <sup>s</sup>	-00 <sup>o</sup> 24 <sup>m</sup> 25.59 <sup>s</sup>	0.5991	14	2	...	...	...	18.50	extended	...
220272017	22 <sup>h</sup> 21 <sup>m</sup> 33.76 <sup>s</sup>	+01 <sup>o</sup> 01 <sup>m</sup> 19.75 <sup>s</sup>	0.5340	14	2	...	...	...	18.99	extended	...
220608343	22 <sup>h</sup> 18 <sup>m</sup> 22.66 <sup>s</sup>	+00 <sup>o</sup> 17 <sup>m</sup> 15.43 <sup>s</sup>	0.5240	14	2	21.01	20.92	20.51	20.25	extended	...
220536609	22 <sup>h</sup> 15 <sup>m</sup> 31.65 <sup>s</sup>	+00 <sup>o</sup> 04 <sup>m</sup> 18.31 <sup>s</sup>	0.4970	14	1	...	...	...	21.09	extended	...
220554336	22 <sup>h</sup> 14 <sup>m</sup> 44.17 <sup>s</sup>	+00 <sup>o</sup> 10 <sup>m</sup> 02.54 <sup>s</sup>	0.4470	14	1	...	...	...	21.02	point-like	...

**Table B.1.** continued.

Object ID (1)	$\alpha_{J2000}$ (2)	$\delta_{J2000}$ (3)	$z$ (4)	Flag (5)	Epoch (6)	$B_{AB}$ (7)	$V_{AB}$ (8)	$R_{AB}$ (9)	$I_{AB}$ (10)	Morphology (11)	Remark (12)
220355666	22 <sup>h</sup> 18 <sup>m</sup> 37.47 <sup>s</sup>	-00 <sup>o</sup> 17 <sup>m</sup> 31.44 <sup>s</sup>	0.4394	14	2	...	...	...	18.01	point-like	...
220209990	22 <sup>h</sup> 19 <sup>m</sup> 34.17 <sup>s</sup>	+00 <sup>o</sup> 39 <sup>m</sup> 12.28 <sup>s</sup>	0.4062	14	2	20.60	20.50	19.69	19.65	extended	...
220493749	22 <sup>h</sup> 16 <sup>m</sup> 08.78 <sup>s</sup>	-00 <sup>o</sup> 11 <sup>m</sup> 42.07 <sup>s</sup>	0.3263	14	2	...	...	...	20.52	point-like	...
220346642	22 <sup>h</sup> 18 <sup>m</sup> 52.40 <sup>s</sup>	-00 <sup>o</sup> 21 <sup>m</sup> 33.62 <sup>s</sup>	0.3145	14	2	...	...	...	18.88	extended	...
220257203	22 <sup>h</sup> 18 <sup>m</sup> 54.37 <sup>s</sup>	+00 <sup>o</sup> 56 <sup>m</sup> 28.06 <sup>s</sup>	0.2513	14	2	...	...	...	18.23	extended	...

Table columns: (1) Object identification number of the VVDS database; (2), (3) Right ascension and declination J2000.0; (4) Redshift; (5) Redshift quality flag. Flag 14 AGN have a 100% secure redshift based on at least two emission lines. Flag 13 AGN have a redshift which is based on one broad emission line with a confident identification: either no other identification is verisimilar given our spectral wavelength coverage, or some faint additional features are supporting the chosen redshift; (6) VVDS observation epoch; (7), (8), (9), (10)  $B$ ,  $V$ ,  $R$ ,  $I$  magnitudes in the AB system. Photometry in the CDFS field is extracted from the EIS catalog (Arnouts et al. 2001) while in the 4 other fields it corresponds to the VVDS imaging survey (McCracken et al. 2003). These magnitudes are corrected for galactic extinction using the dust map provided by Schlegel et al. (1998); (11) Morphological classification in the  $I$ -band, based on the half-light radius of the object. Object with  $I_{AB} > 22.5$  or in the CDFS and VVDS-1400+05 field are not classified (See Gavignaud et al. 2006, Sect. 7); (12) We indicate here, AGN for which a single broad emission line is detected in the VVDS original spectrum but for which a second line is detected at shorter wavelength either in our VIMOS and FORS follow-up programs, or in one of these spectroscopic survey: 2Qz (Croom et al. 2004), SDSS DR6 (Adelman-McCarthy & the SDSS Collaboration 2007), and the spectroscopic catalog of the CDFS (Szokoly et al. 2004).

**Table B.2.** AGN with a single emission line detected (flag 19).

Object ID (1)	$\alpha_{J2000}$ (2)	$\delta_{J2000}$ (3)	Epoch (4)	$\lambda_{BL}$ (5)	$z$ solutions (6)	$B_{AB}$ (7)	$V_{AB}$ (8)	$R_{AB}$ (9)	$I_{AB}$ (10)	Morphology (11)
CDFS: deep mode 2 AGN										
000031270	03 <sup>h</sup> 32 <sup>m</sup> 57.74 <sup>s</sup>	-27 <sup>o</sup> 43 <sup>m</sup> 50.12 <sup>s</sup>	1	7319.	0.1150 <sup>a</sup> 1.6150 <sup>b</sup>	23.81	23.65	23.44	23.52	...
000017025	03 <sup>h</sup> 31 <sup>m</sup> 54.30 <sup>s</sup>	-27 <sup>o</sup> 53 <sup>m</sup> 49.58 <sup>s</sup>	1	6500.	1.3220 <sup>b</sup> 2.4050 <sup>c</sup> 3.1960 <sup>d</sup>	24.78	24.51	23.93	23.70	...
0226-04 : deep mode 6 AGN										
020375508	02 <sup>h</sup> 25 <sup>m</sup> 48.99 <sup>s</sup>	-04 <sup>o</sup> 10 <sup>m</sup> 28.04 <sup>s</sup>	1	5963.	1.1300 <sup>b</sup> 2.1240 <sup>c</sup> 2.8500 <sup>d</sup>	23.25	22.98	23.05	22.54	...
020293248	02 <sup>h</sup> 26 <sup>m</sup> 25.92 <sup>s</sup>	-04 <sup>o</sup> 21 <sup>m</sup> 12.73 <sup>s</sup>	1	7335.	0.1180 <sup>a</sup> 1.6210 <sup>b</sup>	24.79	24.54	24.14	23.26	...
020281035	02 <sup>h</sup> 26 <sup>m</sup> 12.30 <sup>s</sup>	-04 <sup>o</sup> 22 <sup>m</sup> 51.63 <sup>s</sup>	1	6805.	0.0370 <sup>a</sup> 1.4310 <sup>b</sup> 2.5650 <sup>c</sup> 3.3930 <sup>d</sup>	25.07	24.39	24.07	23.93	...
020469530	02 <sup>h</sup> 26 <sup>m</sup> 49.92 <sup>s</sup>	-04 <sup>o</sup> 15 <sup>m</sup> 17.44 <sup>s</sup>	1	6701.	0.0210 <sup>a</sup> 1.3940 <sup>b</sup> 2.5100 <sup>c</sup> 3.3260 <sup>d</sup>	24.69	24.36	24.28	23.50	...
020225567	02 <sup>h</sup> 27 <sup>m</sup> 06.42 <sup>s</sup>	-04 <sup>o</sup> 30 <sup>m</sup> 14.34 <sup>s</sup>	1	6558.	1.3430 <sup>b</sup> 2.4350 <sup>c</sup>	24.65	24.26	23.74	23.07	...
020137737	02 <sup>h</sup> 26 <sup>m</sup> 47.76 <sup>s</sup>	-04 <sup>o</sup> 42 <sup>m</sup> 04.06 <sup>s</sup>	1	6320.	1.2580 <sup>b</sup> 2.3110 <sup>c</sup> 3.0800 <sup>d</sup>	24.59	24.15	24.17	23.78	...
1003+01: Wide mode 5 AGN										
100093239	10 <sup>h</sup> 07 <sup>m</sup> 38.99 <sup>s</sup>	+01 <sup>o</sup> 16 <sup>m</sup> 38.69 <sup>s</sup>	2	7554.	0.1510 <sup>a</sup> 1.7000 <sup>b</sup>	...	...	...	20.29	point-like
100461830	10 <sup>h</sup> 03 <sup>m</sup> 48.70 <sup>s</sup>	+02 <sup>o</sup> 10 <sup>m</sup> 45.16 <sup>s</sup>	2	6700.	0.0210 <sup>a</sup> 1.3950 <sup>b</sup> 2.5100 <sup>c</sup> 3.3250 <sup>d</sup>	21.86	21.78	21.70	21.37	extended
100361479	10 <sup>h</sup> 03 <sup>m</sup> 43.19 <sup>s</sup>	+01 <sup>o</sup> 57 <sup>m</sup> 03.28 <sup>s</sup>	2	6564.	1.3460 <sup>b</sup> 2.4380 <sup>c</sup>	23.11	22.75	22.49	22.10	extended
100393370	10 <sup>h</sup> 03 <sup>m</sup> 36.11 <sup>s</sup>	+02 <sup>o</sup> 01 <sup>m</sup> 30.20 <sup>s</sup>	2	6383.	1.2810 <sup>b</sup> 2.3440 <sup>c</sup>	22.49	22.34	22.68	22.16	point-like
100573419	10 <sup>h</sup> 04 <sup>m</sup> 14.34 <sup>s</sup>	+02 <sup>o</sup> 27 <sup>m</sup> 17.66 <sup>s</sup>	2	6381.	1.2810 <sup>b</sup> 2.3430 <sup>c</sup>	22.86	22.21	22.13	21.78	extended
1400+05: Wide mode 12 AGN										
140421262	13 <sup>h</sup> 58 <sup>m</sup> 39.67 <sup>s</sup>	+05 <sup>o</sup> 09 <sup>m</sup> 40.06 <sup>s</sup>	2	6155.	1.2000 <sup>b</sup> 2.2240 <sup>c</sup> 2.9740 <sup>d</sup>	19.92	19.72	19.60	19.85	...
140242524	13 <sup>h</sup> 55 <sup>m</sup> 50.62 <sup>s</sup>	+04 <sup>o</sup> 42 <sup>m</sup> 21.20 <sup>s</sup>	2	6804.	0.0370 <sup>a</sup> 1.4320 <sup>b</sup> 2.5640 <sup>c</sup>	...	...	...	21.59	...
140304399	14 <sup>h</sup> 01 <sup>m</sup> 25.45 <sup>s</sup>	+04 <sup>o</sup> 51 <sup>m</sup> 27.48 <sup>s</sup>	2	6256.	1.2360 <sup>b</sup> 2.2770 <sup>c</sup>	22.84	22.44	22.20	21.91	...
140361276	13 <sup>h</sup> 50 <sup>m</sup> 29.99 <sup>s</sup>	+04 <sup>o</sup> 59 <sup>m</sup> 32.38 <sup>s</sup>	2	5775.	1.0640 <sup>b</sup> 2.0250 <sup>c</sup>	21.89	21.51	21.73	21.55	...
140242100	14 <sup>h</sup> 00 <sup>m</sup> 33.03 <sup>s</sup>	+04 <sup>o</sup> 42 <sup>m</sup> 22.67 <sup>s</sup>	2	7720.	0.1760 <sup>a</sup> 1.7590 <sup>b</sup>	23.08	22.78	22.42	21.94	...
140364738	13 <sup>h</sup> 58 <sup>m</sup> 17.25 <sup>s</sup>	+04 <sup>o</sup> 59 <sup>m</sup> 56.90 <sup>s</sup>	2	6773.	0.0320 <sup>a</sup> 1.4210 <sup>b</sup> 2.5480 <sup>c</sup>	20.66	20.27	20.00	20.48	...
140450459	13 <sup>h</sup> 58 <sup>m</sup> 33.08 <sup>s</sup>	+05 <sup>o</sup> 14 <sup>m</sup> 40.05 <sup>s</sup>	2	6657.	0.0140 <sup>a</sup> 1.3790 <sup>b</sup> 2.4870 <sup>c</sup>	21.64	21.58	21.35	21.55	...
140387670	13 <sup>h</sup> 59 <sup>m</sup> 22.13 <sup>s</sup>	+05 <sup>o</sup> 03 <sup>m</sup> 53.84 <sup>s</sup>	2	6590.	0.0040 <sup>a</sup> 1.3550 <sup>b</sup> 2.4520 <sup>c</sup>	21.71	21.36	21.11	21.12	...
140268727	13 <sup>h</sup> 59 <sup>m</sup> 46.93 <sup>s</sup>	+04 <sup>o</sup> 46 <sup>m</sup> 14.84 <sup>s</sup>	2	6584.	0.0030 <sup>a</sup> 1.3530 <sup>b</sup> 2.4490 <sup>c</sup>	...	...	19.13	19.22	...
140276121	14 <sup>h</sup> 00 <sup>m</sup> 26.72 <sup>s</sup>	+04 <sup>o</sup> 47 <sup>m</sup> 19.30 <sup>s</sup>	2	6564.	1.3460 <sup>b</sup> 2.4390 <sup>c</sup>	19.87	19.69	19.90	19.85	...
140373173	13 <sup>h</sup> 58 <sup>m</sup> 37.46 <sup>s</sup>	+05 <sup>o</sup> 01 <sup>m</sup> 22.89 <sup>s</sup>	2	6090.	1.1770 <sup>b</sup> 2.1900 <sup>c</sup> 2.9320 <sup>d</sup>	22.56	21.75	21.56	21.76	...
140312115	13 <sup>h</sup> 57 <sup>m</sup> 41.81 <sup>s</sup>	+04 <sup>o</sup> 52 <sup>m</sup> 33.24 <sup>s</sup>	2	6041.	1.1590 <sup>b</sup> 2.1640 <sup>c</sup>	...	...	21.72	22.16	...
2217+00: Wide mode 38 AGN										
220525641	22 <sup>h</sup> 16 <sup>m</sup> 31.69 <sup>s</sup>	+00 <sup>o</sup> 00 <sup>m</sup> 38.07 <sup>s</sup>	2	6874.	0.0470 <sup>a</sup> 1.4570 <sup>b</sup> 2.6010 <sup>c</sup>	21.77	21.69	21.41	21.44	point-like
220266865	22 <sup>h</sup> 20 <sup>m</sup> 50.58 <sup>s</sup>	+00 <sup>o</sup> 59 <sup>m</sup> 48.73 <sup>s</sup>	2	6840.	0.0420 <sup>a</sup> 1.4450 <sup>b</sup> 2.5830 <sup>c</sup> 3.4160 <sup>d</sup>	...	...	...	19.73	point-like
220277254	22 <sup>h</sup> 20 <sup>m</sup> 54.48 <sup>s</sup>	+01 <sup>o</sup> 03 <sup>m</sup> 10.78 <sup>s</sup>	2	6450.	1.3050 <sup>b</sup> 2.3780 <sup>c</sup>	...	...	...	20.91	point-like
220145240	22 <sup>h</sup> 14 <sup>m</sup> 06.83 <sup>s</sup>	+01 <sup>o</sup> 07 <sup>m</sup> 29.30 <sup>s</sup>	2	6364.	1.2750 <sup>b</sup> 2.3340 <sup>c</sup>	...	...	...	22.24	point-like

**Table B.2.** continued.

Object ID (1)	$\alpha_{J2000}$ (2)	$\delta_{J2000}$ (3)	Epoch (4)	$\lambda_{BL}$ (5)	$z$ solutions (6)	$B_{AB}$ (7)	$V_{AB}$ (8)	$R_{AB}$ (9)	$I_{AB}$ (10)	Morphology (11)
220430837	22 <sup>h</sup> 19 <sup>m</sup> 58.43 <sup>s</sup>	+00°16 <sup>m</sup> 30.20 <sup>s</sup>	2	6193.	1.2130 <sup>b</sup> 2.2440 <sup>c</sup>	21.35	21.14	21.06	20.72	extended
220056092	22 <sup>h</sup> 13 <sup>m</sup> 53.81 <sup>s</sup>	+00°41 <sup>m</sup> 06.90 <sup>s</sup>	1	6100.	1.1790 <sup>b</sup> 2.1950 <sup>c</sup>	...	...	...	22.09	point-like
220514141	22 <sup>h</sup> 15 <sup>m</sup> 28.78 <sup>s</sup>	-00°03 <sup>m</sup> 01.29 <sup>s</sup>	2	5956.	1.1290 <sup>b</sup> 2.1200 <sup>c</sup>	...	...	...	22.16	extended
220456500	22 <sup>h</sup> 17 <sup>m</sup> 24.92 <sup>s</sup>	-00°27 <sup>m</sup> 49.19 <sup>s</sup>	2	8524.	0.2990 <sup>a</sup> 0.0460 <sup>b</sup>	...	...	...	22.35	point-like
220551735	22 <sup>h</sup> 18 <sup>m</sup> 05.78 <sup>s</sup>	+00°09 <sup>m</sup> 12.66 <sup>s</sup>	1	8056.	0.2270 <sup>a</sup> 1.8780 <sup>b</sup>	21.73	21.72	21.14	21.12	point-like
220450780	22 <sup>h</sup> 16 <sup>m</sup> 37.41 <sup>s</sup>	-00°30 <sup>m</sup> 27.37 <sup>s</sup>	2	7543.	0.1490 <sup>a</sup> 1.6960 <sup>b</sup>	...	...	...	21.31	extended
220514417	22 <sup>h</sup> 15 <sup>m</sup> 30.67 <sup>s</sup>	-00°02 <sup>m</sup> 57.02 <sup>s</sup>	2	7387.	0.1260 <sup>a</sup> 1.6400 <sup>b</sup>	...	...	...	21.20	point-like
220583713	22 <sup>h</sup> 15 <sup>m</sup> 34.70 <sup>s</sup>	+00°18 <sup>m</sup> 42.01 <sup>s</sup>	1	7352.	0.1200 <sup>a</sup> 1.6270 <sup>b</sup>	...	...	...	21.89	point-like
220153188	22 <sup>h</sup> 15 <sup>m</sup> 42.00 <sup>s</sup>	+01°09 <sup>m</sup> 54.38 <sup>s</sup>	2	7280.	0.1090 <sup>a</sup> 1.6020 <sup>b</sup>	...	...	...	22.00	point-like
220415034	22 <sup>h</sup> 21 <sup>m</sup> 01.42 <sup>s</sup>	+00°09 <sup>m</sup> 11.33 <sup>s</sup>	2	7206.	0.0980 <sup>a</sup> 1.5750 <sup>b</sup>	21.73	21.68	21.40	21.08	point-like
220417000	22 <sup>h</sup> 21 <sup>m</sup> 16.89 <sup>s</sup>	+00°10 <sup>m</sup> 01.43 <sup>s</sup>	2	7181.	0.0940 <sup>a</sup> 1.5660 <sup>b</sup>	22.87	22.40	21.88	21.40	point-like
220442138	22 <sup>h</sup> 21 <sup>m</sup> 02.71 <sup>s</sup>	+00°22 <sup>m</sup> 06.71 <sup>s</sup>	2	7037.	0.0720 <sup>a</sup> 1.5150 <sup>b</sup>	22.15	22.21	21.64	21.47	point-like
220023681	22 <sup>h</sup> 17 <sup>m</sup> 46.44 <sup>s</sup>	+00°31 <sup>m</sup> 26.58 <sup>s</sup>	1	6956.	0.0600 <sup>a</sup> 1.4850 <sup>b</sup> 2.6440 <sup>c</sup>	24.33	23.25	22.14	21.71	point-like
220593613	22 <sup>h</sup> 14 <sup>m</sup> 11.61 <sup>s</sup>	+00°21 <sup>m</sup> 29.15 <sup>s</sup>	1	6893.	0.0500 <sup>a</sup> 1.4630 <sup>b</sup> 2.6110 <sup>c</sup>	...	...	...	21.89	extended
220248236	22 <sup>h</sup> 20 <sup>m</sup> 35.99 <sup>s</sup>	+00°53 <sup>m</sup> 39.78 <sup>s</sup>	2	6787.	0.0340 <sup>a</sup> 1.4260 <sup>b</sup> 2.5550 <sup>c</sup>	...	...	...	21.75	point-like
220548678	22 <sup>h</sup> 15 <sup>m</sup> 02.71 <sup>s</sup>	+00°08 <sup>m</sup> 10.56 <sup>s</sup>	1	6766.	0.0310 <sup>a</sup> 1.4170 <sup>b</sup> 2.5440 <sup>c</sup>	...	...	...	21.98	point-like
220450644	22 <sup>h</sup> 14 <sup>m</sup> 59.31 <sup>s</sup>	-00°30 <sup>m</sup> 32.88 <sup>s</sup>	2	6682.	0.0180 <sup>a</sup> 1.3880 <sup>b</sup> 2.5000 <sup>c</sup>	...	...	...	19.81	point-like
220367657	22 <sup>h</sup> 19 <sup>m</sup> 11.81 <sup>s</sup>	-00°12 <sup>m</sup> 07.27 <sup>s</sup>	2	6642.	0.0120 <sup>a</sup> 1.3740 <sup>b</sup> 2.4790 <sup>c</sup>	...	20.89	...	20.44	extended
220340940	22 <sup>h</sup> 19 <sup>m</sup> 55.93 <sup>s</sup>	-00°24 <sup>m</sup> 12.15 <sup>s</sup>	2	6627.	0.0100 <sup>a</sup> 1.3690 <sup>b</sup> 2.4720 <sup>c</sup>	...	...	...	21.19	point-like
220528506	22 <sup>h</sup> 17 <sup>m</sup> 14.92 <sup>s</sup>	+00°01 <sup>m</sup> 34.79 <sup>s</sup>	2	6625.	0.0090 <sup>a</sup> 1.3680 <sup>b</sup> 2.4700 <sup>c</sup>	21.70	21.70	21.70	21.42	extended
220293272	22 <sup>h</sup> 19 <sup>m</sup> 51.69 <sup>s</sup>	+01°08 <sup>m</sup> 34.19 <sup>s</sup>	2	6600.	0.0060 <sup>a</sup> 1.3590 <sup>b</sup> 2.4570 <sup>c</sup>	...	...	...	20.20	point-like
220416619	22 <sup>h</sup> 21 <sup>m</sup> 00.87 <sup>s</sup>	+00°09 <sup>m</sup> 51.78 <sup>s</sup>	2	6586.	0.0040 <sup>a</sup> 1.3540 <sup>b</sup> 2.4500 <sup>c</sup>	21.87	21.70	21.63	21.41	point-like
220450790	22 <sup>h</sup> 16 <sup>m</sup> 36.78 <sup>s</sup>	-00°30 <sup>m</sup> 25.92 <sup>s</sup>	2	6574.	0.0020 <sup>a</sup> 1.3490 <sup>b</sup> 2.4440 <sup>c</sup>	...	...	...	21.84	point-like
220417927	22 <sup>h</sup> 20 <sup>m</sup> 52.10 <sup>s</sup>	+00°10 <sup>m</sup> 25.42 <sup>s</sup>	2	6574.	0.0020 <sup>a</sup> 1.3490 <sup>b</sup> 2.4430 <sup>c</sup>	22.26	22.05	21.70	21.23	point-like
220527985	22 <sup>h</sup> 17 <sup>m</sup> 48.67 <sup>s</sup>	+00°01 <sup>m</sup> 25.97 <sup>s</sup>	2	6546.	1.3390 <sup>b</sup> 2.4290 <sup>c</sup>	21.97	22.02	21.50	21.82	point-like
220260114	22 <sup>h</sup> 18 <sup>m</sup> 52.63 <sup>s</sup>	+00°57 <sup>m</sup> 40.38 <sup>s</sup>	2	6467.	1.3110 <sup>b</sup> 2.3880 <sup>c</sup>	...	...	...	21.98	point-like
220234909	22 <sup>h</sup> 18 <sup>m</sup> 13.40 <sup>s</sup>	+00°48 <sup>m</sup> 54.05 <sup>s</sup>	1	6407.	1.2890 <sup>b</sup> 2.3560 <sup>c</sup> 3.1360 <sup>d</sup>	23.40	22.55	21.99	21.88	extended
220457558	22 <sup>h</sup> 15 <sup>m</sup> 42.94 <sup>s</sup>	-00°27 <sup>m</sup> 21.12 <sup>s</sup>	2	6378.	1.2790 <sup>b</sup> 2.3410 <sup>c</sup>	...	...	...	22.10	point-like
220216575	22 <sup>h</sup> 20 <sup>m</sup> 02.85 <sup>s</sup>	+00°41 <sup>m</sup> 50.22 <sup>s</sup>	2	6361.	1.2730 <sup>b</sup> 2.3320 <sup>c</sup> 3.1070 <sup>d</sup>	21.43	21.43	21.20	21.31	point-like
220515291	22 <sup>h</sup> 18 <sup>m</sup> 02.63 <sup>s</sup>	-00°02 <sup>m</sup> 39.74 <sup>s</sup>	2	6319.	1.2580 <sup>b</sup> 2.3100 <sup>c</sup>	23.15	23.14	22.57	21.87	extended
220442069	22 <sup>h</sup> 21 <sup>m</sup> 03.65 <sup>s</sup>	+00°22 <sup>m</sup> 04.02 <sup>s</sup>	2	6119.	1.1870 <sup>b</sup> 2.2050 <sup>c</sup>	21.39	21.25	21.28	21.03	point-like
220399800	22 <sup>h</sup> 20 <sup>m</sup> 14.86 <sup>s</sup>	+00°02 <sup>m</sup> 46.33 <sup>s</sup>	2	6092.	1.1770 <sup>b</sup> 2.1910 <sup>c</sup>	22.76	22.30	22.03	21.96	extended
220608923	22 <sup>h</sup> 18 <sup>m</sup> 33.29 <sup>s</sup>	+00°18 <sup>m</sup> 35.17 <sup>s</sup>	2	6007.	1.1470 <sup>b</sup> 2.1470 <sup>c</sup>	22.01	21.58	21.14	21.58	point-like
220371718	22 <sup>h</sup> 18 <sup>m</sup> 15.48 <sup>s</sup>	-00°10 <sup>m</sup> 19.03 <sup>s</sup>	2	5984.	1.1390 <sup>b</sup> 2.1350 <sup>c</sup>	...	21.95	...	21.67	point-like

Table columns: (1) Object identification number of the VVDS database; (2), (3) Right ascension and declination J2000.0; (4) VVDS observation epoch; (5), (6) Observed wavelength of the broad-emission line and possible redshifts. Superscript indicate the identifications for the emission line: *a*, *b*, *c*, *d* respectively correspond to H $\alpha$ , Mg II, C III, and C IV; (7), (8), (9), (10) *B*, *V*, *R*, *I* magnitudes in the AB system (see Table B.1); (11) Morphological classification in the *I*-band (see Table B.1).

## References

- Adelman-McCarthy, J. K., & the SDSS Collaboration. 2007, ArXiv e-prints, 707
- Arnouts, S., Vandame, B., Benoist, C., et al. 2001, A&A, 379, 740
- Babić, A., Miller, L., Jarvis, M. J., et al. 2007, A&A, 474, 755
- Baskin, A., & Laor, A. 2005, MNRAS, 356, 1029
- Bentz, M. C., Peterson, B. M., Pogge, R. W., Vestergaard, M., & Onken, C. A. 2006, ApJ, 644, 133
- Bongiorno, A., Zamorani, G., Gavignaud, I., et al. 2007, A&A, 472, 443
- Cattaneo, A. 2001, MNRAS, 324, 128
- Collin, S., Kawaguchi, T., Peterson, B. M., & Vestergaard, M. 2006, A&A, 456, 75
- Croom, S. M., Smith, R. J., Boyle, B. J., et al. 2004, MNRAS, 349, 1397
- Ferrarese, L., & Merritt, D. 2000, ApJ, 539, L9
- Fine, S., Croom, S. M., Hopkins, P. F., et al. 2008, ArXiv e-prints, 807
- Garilli, B., Le Fèvre, O., Guzzo, L., et al. 2008, ArXiv e-prints, 804
- Gaskell, C. M. 1982, ApJ, 263, 79
- Gavignaud, I., Bongiorno, A., Paltani, S., et al. 2006, A&A, 457, 79
- Gebhardt, K., Bender, R., Bower, G., et al. 2000, ApJ, 539, L13
- Hasinger, G., Miyaji, T., & Schmidt, M. 2005, A&A, 441, 417
- Hopkins, P. F., Hernquist, L., Cox, T. J., et al. 2006, ApJ, 639, 700
- Hopkins, P. F., Richards, G. T., & Hernquist, L. 2007, ApJ, 654, 731
- Kaspi, S., Brandt, W. N., Maoz, D., et al. 2007, ApJ, 659, 997
- Kollmeier, J. A., Onken, C. A., Kochanek, C. S., et al. 2006, ApJ, 648, 128
- Le Fèvre, O., Vettolani, G., Garilli, B., et al. 2005, A&A, 439, 845
- Marconi, A., Risaliti, G., Gilli, R., et al. 2004, MNRAS, 351, 169
- Marconi, A., Axon, D. J., Maiolino, R., et al. 2008, ApJ, 678, 693
- McCracken, H. J., Radovich, M., Bertin, E., et al. 2003, A&A, 410, 17
- McLure, R. J., & Dunlop, J. S. 2004, MNRAS, 352, 1390
- McLure, R. J., & Jarvis, M. J. 2002, MNRAS, 337, 109
- Netzer, H., Lira, P., Trakhtenbrot, B., Shemmer, O., & Cury, I. 2007, ApJ, 671, 1256
- Paltani, S., & Türler, M. 2005, A&A, 435, 811
- Richards, G. T., Fan, X., Newberg, H. J., et al. 2002, AJ, 123, 2945
- Richards, G. T., Strauss, M. A., Fan, X., et al. 2006, AJ, 131, 2766
- Schlegel, D. J., Finkbeiner, D. P., & Davis, M. 1998, ApJ, 500, 525
- Shen, Y., Greene, J. E., Strauss, M. A., Richards, G. T., & Schneider, D. P. 2008, ApJ, 680, 169
- Sigut, T. A. A., & Pradhan, A. K. 2003, ApJS, 145, 15
- Soltan, A. 1982, MNRAS, 200, 115
- Steffen, A. T., Stratova, I., Brandt, W. N., et al. 2006, AJ, 131, 2826
- Szokoly, G. P., Bergeron, J., Hasinger, G., et al. 2004, ApJS, 155, 271
- Tytler, D., & Fan, X.-M. 1992, ApJS, 79, 1
- Vestergaard, M. 2002, ApJ, 571, 733
- Vestergaard, M., & Peterson, B. M. 2006, ApJ, 641, 689
- Vestergaard, M., & Wilkes, B. J. 2001, ApJS, 134, 1
- Wolf, C., Wisotzki, L., Borch, A., et al. 2003, A&A, 408, 499
- Woo, J.-H., & Urry, C. M. 2002, ApJ, 579, 530
- Yu, Q., & Tremaine, S. 2002, MNRAS, 335, 965